Phase diagram of the correlated quarter-filled-band organic salt series (o-DMTTF)$_2X$ (X = Cl, Br, I)

P. Foury-Leylekian,[1,*] P. Auban-Senzier,[1] C. Coulon,[2] O. Jeannin,[3] M. Fourmigué,[3] C. Pasquier,[1] and J.-P. Pouget[1]

[1]*Laboratoire de Physique des Solides, Université Paris Sud, CNRS, UMR 8502, 91405 Orsay, France*

[2]*Université Bordeaux 1, Centre de Recherche Paul Pascal, CNRS, UPR CNRS 8641, 115 Avenue Dr. A. Schweitzer, 33600 Pessac, France*

[3]*Sciences Chimiques de Rennes, Université de Rennes 1, UMR CNRS 6226, Campus de Beaulieu, 35042 Rennes, France*

(Received 30 June 2011; revised manuscript received 2 September 2011; published 28 November 2011)

The 2:1 family of organic salts (o-DMTTF)$_2X$ (X = Cl, Br, I) exhibits regular stacks and a high-symmetry structure, which provide a perfect three-quarter-filling-band system allowing a rich phase diagram in the presence of strong electronic correlations. In this paper, we present a detailed study of this series combining complementary experimental techniques such as resistivity, thermopower, electron spin resonance, static magnetic measurements, and x-ray diffraction. In particular, we show that at ambient pressure (o-DMTTF)$_2X$ with X = Br and Cl undergoes two successive phase transitions setting successively a $4k_F$ charge density and bond order wave order, then a spin-Peierls (SP) ground state. We discuss the symmetry of these phases and its relationship with the transport and magnetic properties. These phases are also followed under pressure by transport experiments, allowing the establishment of a generic phase diagram for this series of salts, where, with the onset of a one-dimensional to three-dimensional deconfinement transition, the $4k_F$ order vanishes and the SP ground state transforms into a Peierls one. Interestingly, this phase diagram differs significantly from the one previously reported in other three-quarter-filled systems such as (TMTTF)$_2X$ and δ-(EDT-TTF-CONMe$_2$)$_2X$.

DOI: 10.1103/PhysRevB.84.195134 PACS number(s): 71.27.+a, 75.25.Dk, 72.80.Le, 71.30.+h

I. INTRODUCTION

The physics of one-dimensional (1D) conductors remains extremely rich because their reduced electronic dimensionality allows a subtle interplay between electronic, magnetic, and lattice degrees of freedom.[1–3] Among these systems, organic materials are of special interest because they exhibit both strong and long-range electron-electron repulsions. Indeed, *ab initio* calculations recently show that the Coulomb repulsion coupling (intrasite U and intersite V_i interactions) are significantly larger than the intrastack transfer integral t and that V_i decreases smoothly with the intersite distance d_i, where d is the stack periodicity.[4] These peculiar features lead to the observation that many partially filled organic systems exhibit an electronic instability toward a generalized Wigner localization,[5] when coupling with the lattice gives rise to the so-called $4k_F$ instability probed in early research by x-ray diffuse scattering techniques.[6] This instability depends significantly upon the band filling. It is enhanced in half-filled and quarter-filled materials because in these cases only strong U and strong U, V_1 are, respectively, required to achieve the electron localization. However as U and V_1 are also sensitive to the polarizability of the organic molecules and to the screening due to the environment of the organic stack,[7] the magnitude of the $4k_F$ localization depends upon the molecular material.

In half-filled-band systems, U induces the well-known Mott-Hubbard localization of one carrier every site. This leads to an efficient decoupling of charge and spin degrees of freedom. At low temperature the spin-1/2 couple antiferromagnetically, which drives the system either to an antiferromagnetic (AF) order or, in the presence of a strong enough spin-phonon coupling, to a singlet spin-Peierls (SP) ground state, first observed in TTF-CuBDT.[8] However if there is a sizeable near-neighbor Coulomb interaction V_1, this phase diagram can be noticeably modified.[9] For $U < 2V_1$ the Mott-Hubbard ground state is replaced by a $2k_F$ ($=d^*/2$) charge density wave (CDW) phase, presenting in the stack direction an alternation of doubly occupied and empty sites. In this phase the double occupancy leads to a singlet spin pairing, and there is no more decoupling between the charge and spin degrees of freedom. More interestingly, it is predicted for $U \sim 2V_1$ and for U and V_1 interactions below a bicritical point, a narrow $2k_F$ bond order wave (BOW) phase, in which the bond distance is modulated with the p symmetry. In the case of half-band filling, the $2k_F$ BOW and $2k_F$ CDW phases, which have different inversion symmetry, are separated by a phase boundary. In the presence of a staggered site potential (coming from the anionic or cationic sublattice, for example), the CDW instability is favored and leads to a neutral-ionic transition. In the presence of a crystallographic stack dimerization, the $2k_F$ BOW instability is favored and leads to a $2k_F$ Peierls insulating ground state in which the excess and defect of charges alternate along the bonds with a p symmetry. *Ab-initio* calculations[4] suggest that the organic systems could fulfill the condition $U \leqslant 2V_1$. In this respect it has been proposed that alkali-TCNQ salts could exhibit the $2k_F$ BOW phase,[10] and it is found that (TTM-TTP)I$_3$ undergoes a $2k_F$ CDW instability induced by the iodine displacement.[11]

In quarter-filled systems, with one carrier at every two sites, intense Coulomb repulsions extending to several neighbors also induce charge localization.[12,13] By quantifying these interactions by the Tomonaga-Luttinger parameter K_ρ, depending on both U and V_i, the charge-localized insulating ground state occurs for $K_\rho \leqslant 1/4$. For $V_1 > 2V_2$ this phase corresponds to a $4k_F$ CDW or site charge order (CO) with a carrier localized at every two sites, while for $V_1 < 2V_2$ this phase corresponds to a $2k_F$ CDW order with the two first-neighbor sites occupied, followed by two empty sites.[5,14] *Ab-initio* calculations[4] show that in the organic systems $V_1 \sim 2V_2$. For $1 \geqslant K_\rho > 1/4$ the system stays in a Tomonaga-Luttinger metallic state. For $K_\rho \leqslant 1/2$ this electron gas exhibits a $4k_F$ CDW instability, which, when strongly coupled to acoustic phonons, drives the system to a $4k_F$ BOW (or dimer Mott, DM) insulating ground state.[15] Note that for a quarter-filled system, these $4k_F$ CO and DM ground states (named generally "$4k_F$ orders" in the following) have a different symmetry

of inversion. In these ground states, there is decoupling between charge and spin degrees of freedom, and, as for the half-filled systems, the coupling between the $S = \frac{1}{2}$ spins leads either to an AF order or to a SP-$2k_F$ bond order in the presence of a significant coupling with the acoustic phonons. In the $(TMTSF)_2X$ (X being a monovalent anion) Bechgaard salts, $(TMTTF)_2X$ Fabre salts,[16] as well as in the TMTSF-DMTCNQ charge transfer salt,[17] K_ρ found to be close to 1/4. $4k_F$ CO and DM insulating states followed by a SP ground state are, respectively, observed in $(TMTTF)_2PF_6$ and AsF_6[18–20] and in $MEM(TCNQ)_2$.[21] A $4k_F$ CO ground state followed by an AF order is observed in $(TMTTF)_2SbF_6$[22] and in δ-(EDT-TTF-$CONMe_2)_2X$.[23] In the presence of an incipient stack dimerization, the CO state is destabilized with respect to the DM one,[15,24] while the coupling of the stacks to a staggered site potential (due to the anions, for example) enhances the CO.[25] A $4k_F$ CO accompanied by an anion displacement has been recently evidenced in $(TMTTF)_2PF_6$[26,27] and in δ-(EDT-TTF-$CONMe_2)_2Br$.[28] For weaker Coulomb repulsions ($1 \geqslant K_\rho > 1/2$), the divergence of the $2k_F$ CDW or $2k_F$ SDW response function leads, respectively, to $2k_F$ CDW/BOW (Peierls) or $2k_F$ SDW ground states.[1,2] Peierls transitions are observed in organic systems built with more polarizable molecules such as $(FA)_2PF_6$[29] and $(TSeT)_2Cl$.[30] In addition the coupling of the charge instability of the electron gas with the orientational and translational degrees of freedom of the anion sublattice helps to stabilize the $2k_F$ CDW (+BOW when coupled to the acoustic phonons) insulating ground state, as observed at the anion ordering (AO) transitions of $(TMTSF)_2ReO_4$[31] and of $(EDO\text{-}TTF)_2PF_6$.[32]

If the intrastack Coulomb parameters are a key ingredient toward electron localization, other interactions such as the interstack coupling play an important role to specify the nature of the $4k_F$ phases. For instance, with similar values of U and V_1,[4] $(TMTTF)_2X$ stabilizes a CO, while the $MEM(TCNQ)_2$ stabilizes a DM order. The difference could be due to a stronger coupling with the anion sublattice in the former salt in which the interaction is expected to discriminate the site occupancy. In the case of $(DI\text{-}DCNQI)_2Ag$, a mixture of CO and DM orders is observed (see below) and different phasing could be due to the minimization of the interstack Coulomb interactions between localized charges.[33]

Another noticeable feature is that most of the 2:1 quarter-filled salts studied until now, possess stacks presenting a sizeable crystallographic "$4k_F$ bond dimerization." This leads to a conduction band splitting ($2\Delta_b$) and to a half-filled upper conduction band. If one considers only this upper band, one recovers the physics of half-filled systems previously considered. On a theoretical basis, the dimerization induces (via the band splitting $2\Delta_b$) an additional Umklapp $4k_F$ term in the e-e interaction scheme of the 1D electron gas.[12] It leads to the creation of a gap Δ_ρ in the charge degrees of freedom whose magnitude can be sizeable if both Δ_b and the Coulomb repulsions are important.[34] In the temperature range of interest ($T < 300$ K), the charge degrees of freedom are frozen if Δ_ρ is the dominant energy scale (i.e., if $\Delta_\rho > \pi k_B T \sim 0.1$ eV). In that case, the 2:1 salt (classified as type II in Ref. 35) must be considered as half filled. Typical examples are $(DIMET)_2SbF_6$[36] and $(t\text{-}TTF)_2Br$,[37] which exhibit an AF ground state and $(BCP\text{-}TTF)_2PF_6$ and AsF_6,[38] which exhibit a SP ground state. If $\Delta_\rho < 0.1$ eV, or equivalently if the charge localization phenomena due to the dimerization manifests on the conductivity below $T_\rho < 300$ K, the charge degrees of freedom cannot be ignored and the 2:1 salt (of type I in Ref. 35) must be considered as quarter filled. This is the case for $(TMTTF)_2X$ in which $T_\rho \sim 200$ K and high-temperature transport data are well fitted by a quarter-filled model.[16] As previously discussed, these salts exhibit a $4k_F$ CO-ferroelectric transition with a disproportionation of charge between the two molecules of the dimer.[18,19,27]

In order to avoid the complications due to the stack dimerization, a special effort was undertaken to synthesize 2:1 quarter-filled salts with a regular stacking of organic molecules. The first well-studied family was the $(R_1R_2\text{-}DCNQI)_2X$ series,[39] where R_1, R_2 is either a halogen atom or a methyl group. For $X =$ Li or Ag, one gets an electron quarter-filled band. In particular, $(DMe\text{-}DCNQI)_2Ag$ ($R_1 = R_2 =$ Me) presents high-temperature $4k_F$ and $2k_F$ structural instabilities, diverging successively into a $4k_F$ order just followed by a $2k_F$ SP-like transition.[40–42] The compound $(DI\text{-}DCNQI)_2Ag$ ($R_1 = R_2 =$ I) exhibits also a high-temperature 1D $4k_F$ structural instability diverging into a $4k_F$ order[43] but stabilizes an AF ground state at lower temperature.[44–46] However, a recent synchrotron study[33] has revealed the occurrence of a complex $4k_F$ modulation pattern consisting of three types of $4k_F$ order: one with charges on the sites (CO), one with charges on the bonds (DM), and one chain with the presence of charges on both sites and bonds. Finally, the δ-(EDT-TTF-$CONMe_2)_2X$ family appears to be a quarter-filled material based on its average structure determination.[47] However, an accurate determination of the structure of the CO state, already present at room temperature and ambient pressure, revealed that the stacks are in fact weakly dimerized[28] and thus that δ-(EDT-TTF-$CONMe_2)_2X$ exhibits also a weak DM contribution at the $4k_F$ order. When the $4k_F$ localized state is suppressed under pressure, this system stabilizes a low-temperature nonmagnetic insulating state, which could be of the Peierls type.[23] The restoration of a $2k_F$ BOW ground state has to be associated with the suppression of the low-pressure heteropolar charge configurations present in $4k_F$ CO.[15,48] The transition from a $4k_F$ correlated ground state to a Peierls one could also be understood if a deconfinement transition occurs under pressure, as first proposed for half-filled-band materials.[49] Indeed, a zero-temperature transition may occur from a Mott insulating state at low pressure toward a two-dimensional (2D) or three-dimensional (3D) metal at larger pressure, where nesting effects of a warped Fermi surface may stabilize an insulating $2k_F$ CDW/BOW or SDW ground state. Such a model has been also applied to the phase diagram under pressure of the $(TMTTF)_2X$.[52] More recently, in the presence of CO in the low-pressure range, the phase diagrams under pressure of $(DI\text{-}DCNQI)_2Ag$[45,46] and of δ-(EDT-TTF-$CONMe_2)_2X$[23] were also interpreted in this framework.

In this paper, we focus our attention on another 2:1 family of regular stacks, $(o\text{-}DMTTF)_2X$, where the molecule o-DMTTF (*ortho*-dimethyltetrathiafulvalene), hybrid between TTF and TMTTF molecules, possesses only two methyl groups attached to one end of the TTF core. It appears important to revisit the physics of this family, first synthesized in the early 1980s,[50] in particular due to its original and very high-symmetry space group $I\bar{4}2d$.[51] This high symmetry is provided by the

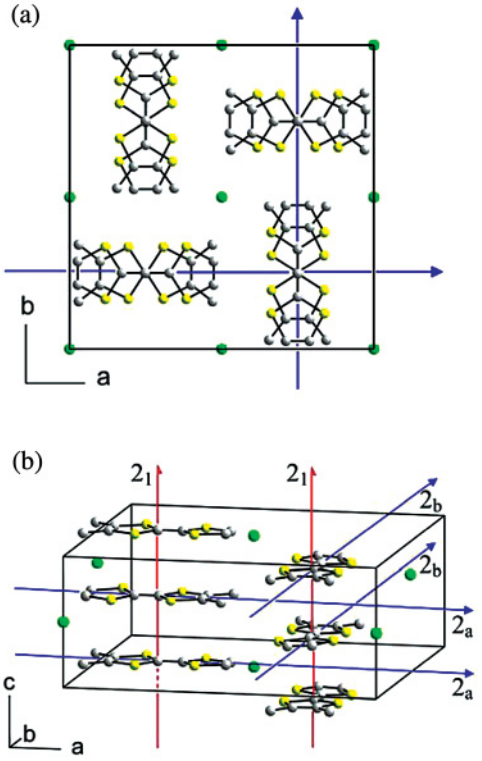

FIG. 1. (Color online) Crystallographic structure of (o-DMTTF)$_2$Cl indicating some symmetry operations of the $I\bar{4}2d$ space group. (a) Projection view along the stacking axis c showing some of the twofold axes. (b) Perspective view showing the 2_1 screw axes along c at the origin of the nondimerized stacks and the two orthogonal sets of twofold axes along a and b (see text).

central position of halogen atoms, X = Cl, Br, I, leading to a strictly uniform stacking and a very weak coupling between first-neighbor orthogonal stacks (Fig. 1). Here, we combine experimental techniques: resistivity, thermopower, electron spin resonance (ESR), static magnetic measurements, and x-ray diffraction in order to get a consistent picture of the low-temperature ground states stabilized in this family. Then we propose a generic phase diagram to unify the various results obtained.

II. EXPERIMENTAL DETAILS

Single crystals of the (o-DMTTF)$_2X$ series have been prepared following the procedure described in Ref. 51. The typical sizes of the needles used were about 0.05–0.2 × 0.05–0.2 × 1–2 mm^3 along the a-, b-, and c-axes for all types of experiments. The measurements were performed on different samples issued from the same batches.

For resistivity measurements, in order to improve the quality of the contacts, gold pads were evaporated on the surface of the crystals before attaching gold wires with silver paste. Standard four-point techniques were used for both measurements of the longitudinal, $\rho_{//}$, and of the transverse, $\rho_{\perp}$, resistivities. For low resistances, a standard low frequency ac lock-in technique was used with applied current, $I_{ac} \approx 0.1$–10 μA. For resistances larger than 50 kΩ, dc measurements were performed with $I_{dc} \approx 0.001$–1 μA.

Resistivity measurements were also performed under high hydrostatic pressure in the longitudinal configuration for the three salts and in the transverse configuration only for the Br salt. For this purpose, a CuBe clamped cell and a NiCrAl clamped cell were used for pressures up to 12 and 23 kbar, respectively, with silicon oil (Daphne 7373) as the pressure transmitting medium. At room temperature, pressure was extracted from the resistance of a manganin gauge in the pressure cell. The loss of pressure during cooling is estimated to 2 kbar. The pressure data were corrected for this loss. A copper-constantan thermocouple inside the pressure cell was used as the thermometer. The resistivity measurements were performed either in a Helium bottle insert in order to reach 5 K or in cryocooler equipment down to 20 K. Longitudinal differential conductance measurements were performed by adding a small low frequency ac voltage to the applied dc voltage, whereas the resulting ac current was measured with a lock-in.

Thermopower (TEP) has been measured at ambient pressure along the stacking axis using a low-frequency ac method (f = 0.01–0.05 Hz) already described elsewhere.[52] Heating one end of the sample was achieved through a commercially available surface mounted chip (SMC) resistor, used as a heater, thermally connected to the sample by a spring-shaped gold wire to avoid mechanical strain. The temperature gradient ranging from 0.3 to 1 K, depending on the temperature, was measured by a chromel-constantan differential thermocouple, whereas the voltage drop was measured with a nanovoltmeter. The sample temperature was measured with a copper-constantan thermocouple connected to the cold end of the sample. TEP experiments have been conducted in vacuum with cryocooler equipment down to 20 K.

ESR experiments were made with a Bruker X-band spectrometer (operating at a microwave frequency of 9.3 GHz) equipped with an ESR 900 Oxford cryostat (allowing exploration of temperatures between 3.8 and 300 K). Selected single crystals were oriented on a quartz rod to study chosen orientations of the crystals relative to the magnetic field. In coherence with the room-temperature crystal structure, a degeneracy was found in the plane perpendicular to the chain axis, and all the information on the ESR signal can be given comparing the orientation along or perpendicular to the chain axis (labeled, respectively, as parallel and perpendicular in the following). This degeneracy has been observed in the whole temperature range, indicating that any departure from the uniaxial symmetry at low temperature remains too weak to be observed. For the presentation of the ESR linewidth data, the correction due the asymmetry of the line has been performed.

To supplement ESR data, magnetic measurements were performed on polycrystalline samples (of typically 10 to 30 mg) with a Quantum Design MPMS-XL superconducting quantum interference device (SQUID) magnetometer in the temperature range 1.8–300 K and up to 70 kOe. Samples were packed in a polyethylene plastic bag (of about 3 × 0.5 × 0.02 cm^3). Experimental data were corrected from the plastic bag, and for the core diamagnetic contribution calculated from Pascal constants. The influence of very small amount of ferromagnetic impurities was also subtracted considering the data measured under different applied magnetic fields.

X-ray diffuse scattering investigation has been performed using a homemade three-circle diffractometer (normal beam geometry with a lifting linear Ar-CH_4 gas detector) equipped with a three-stage closed-circuit He gas cryocooler operating from room temperature down to 1.8 K. The rotation of the sample was provided by a magnetic coupling system connected to the cryocooler head. The experimental setup was mounted on a rotating anode x-ray generator operating at 50 kV, 50 mA, and providing the Cu-K_α ($\lambda = 0.1542$ nm) radiation after Confocal Max-Flux optics (beam size ≈ 350 μm). Before the quantitative measurements, a preliminary photographic investigation using an image plate instead of the linear detector has been systematically performed in order to easily detect additional diffuse scattering or satellite reflections associated with any structural modification. One sample of the Cl salt and two samples of the Br and I salts were investigated.

III. RESULTS

A. Transport measurements

We first present the resistivity data under pressure that will define the main lines of the phase diagram. At ambient pressure, the room-temperature conductivity along the stacking direction (c-axis) is estimated to $\sigma_c = \sigma_{//} = 200$ S.cm^{-1} ($\rho_{//} = 5$ mΩ.cm) for all three compounds. This value is obtained for samples with small sections ($\approx 50 \times 50$ μm^2). For larger samples, the conductivity estimated from the resistance is lower and decreases when the section increases, indicating that the current does not flow through the whole section of the sample, despite gold evaporations all around the needles. A metallic behavior is observed upon cooling, but the occurrence of many microcracks in the sample, a common feature in 1D molecular conductors at ambient pressure, prevented us from getting a reliable curve down to low temperatures. A small applied hydrostatic pressure is enough to get resistivity curves free from jumps due to microcracks.

At ambient pressure, the room-temperature value of the transverse conductivity ($\sigma_a = \sigma_b = \sigma_\perp$) slightly differs between the three compounds from 1.00 to 0.3 S.cm^{-1} ($\rho_\perp = 1$–3 Ω.cm) which leads to an anisotropy, $\sigma_{//}/\sigma_\perp$, which lies between 200 and 700. Upon cooling the samples, a weak localization is observed for $\rho_\perp$, which confirms the 1D nature of the electronic transport.[53] A transition toward an insulating state takes place at low temperature, in two steps for the Cl salt and only one step for the I salt (Fig. 2). The temperatures of the transitions are extracted from the position of the peak in the d(ln ρ)/d(1/T) curves. Although two distinct peaks are visible at 80 and 45 K for the Cl salt, only one broad peak centered at 57 K is visible for the I salt. For the Br salt, the situation is not clear from this measurement, but the occurrence of two transitions at temperatures close to each other will be more visible under pressure (see below).

At room temperature, the pressure dependence of the longitudinal conductivity is linear (inset Fig. 2 for the Cl salt) with a slope $[\sigma_{//}(\mathrm{P}) - \sigma_{//}(1\ \mathrm{bar})]/\sigma_{//}(1\ \mathrm{bar}) \approx +30\%/\mathrm{kbar}$ for all three compounds, which compares fairly well with the (TMTTF)$_2X$ and (TMTSF)$_2X$ salts behavior in the metallic regime.

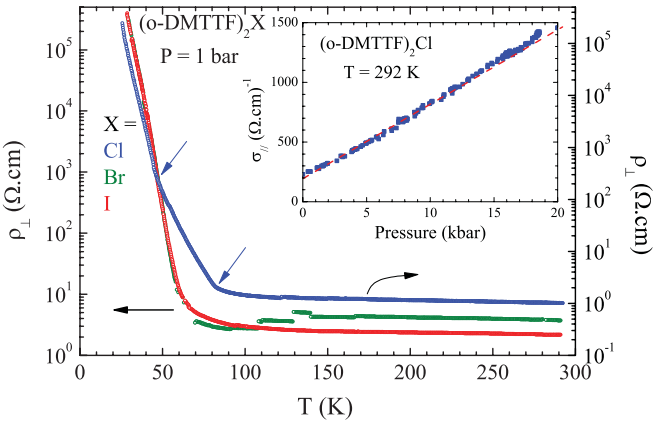

FIG. 2. (Color online) Transverse resistivity as a function of temperature for the (o-DMTTF)$_2X$ series at ambient pressure. Insert: evolution of the room-temperature longitudinal conductivity with pressure in (o-DMTTF)$_2$Cl.

The temperature dependence of the longitudinal resistivity, $\rho_{//}$, for different applied pressures is shown in Figs. 3(a) and 3(b) for two different Cl samples under low and high pressures, respectively. First, a smooth localization is observed below the temperature T_ρ corresponding to the minimum value of the resistivity and whose value decreases with pressure. When cooling down below T_ρ, two successive changes of slope are visible at low pressure (below 6 kbar) in agreement with the ambient pressure $\rho_\perp$(T) data. The upper transition temperature, denoted T_u, decreases with pressure starting from 80 K at low pressure while the lowest transition temperature, denoted T_c, slightly increases. These two transitions seem to merge into a unique transition just above 6 kbar around 50 K. Then, the unique transition temperature decreases from 50 K down to 26 K at 18 kbar, and T_ρ is no longer identified in this pressure range. These evolutions are clearly revealed on the derivative plot d**(**ln(ρ)**)**/d(1/T) versus 1/T shown in the inserts of Fig. 3.

Similar features have been observed in the Br salt. For the lowest pressure [Fig. 4(a)], the longitudinal resistivity presents a minimum at $T_\rho \approx 100$ K, then a first kink around 60 K, followed by a second one around 50 K, similar to the observations made in the Cl salt at low pressure. Comparing the $\rho_{//}$(T) behaviors of the two salts in the whole studied pressure range [Figs. 3 and 4(a) and inserts], we can infer that the properties of the Br salt mimic those of the Cl salt with a pressure shift of 3.5 kbar.

Transverse resistivity, $\rho_\perp$, measurements under pressure have also been performed on the Br salt [Fig. 4(b)] and lead to the same conclusion for the pressure dependence of T_u and T_c. Below 5 kbar, $\rho_\perp$ exhibits a localization behavior at all temperatures. Above 5 kbar, a weak maximum of the resistivity occurs between 200 and 300 K at a temperature denoted T^* whose value increases with pressure. Despite very close values, this temperature can be distinguished from the solidification of the pressure medium (Daphne oil 7373). This solidification is visible as a small bump on both longitudinal and transverse resistivity curves between 180 and 250 K at a temperature also increasing with pressure and in agreement with previous reports.[54] This coincidence leads us to put large error bars in

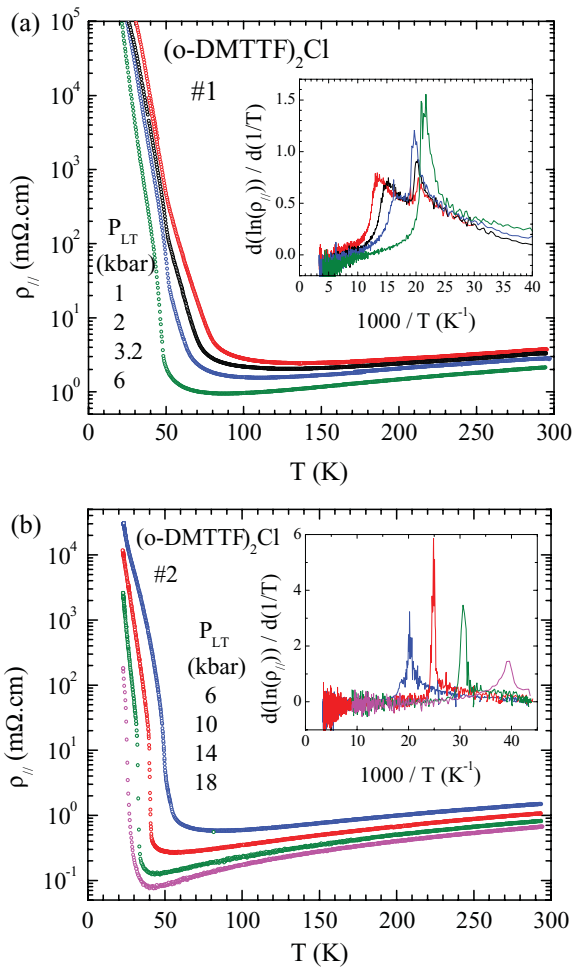

FIG. 3. (Color online) Evolution of the longitudinal resistivity versus temperature in (o-DMTTF)$_2$Cl as a function of hydrostatic pressure (a) at low pressure for sample 1 (b) at high pressure for sample 2. Inserts: d(ln(ρ))/d(1/T) as a function of temperature for all pressures. The characteristic temperatures T_c and T_u of Fig. 16 correspond to the positions of the right and left (if it exists) peaks, respectively.

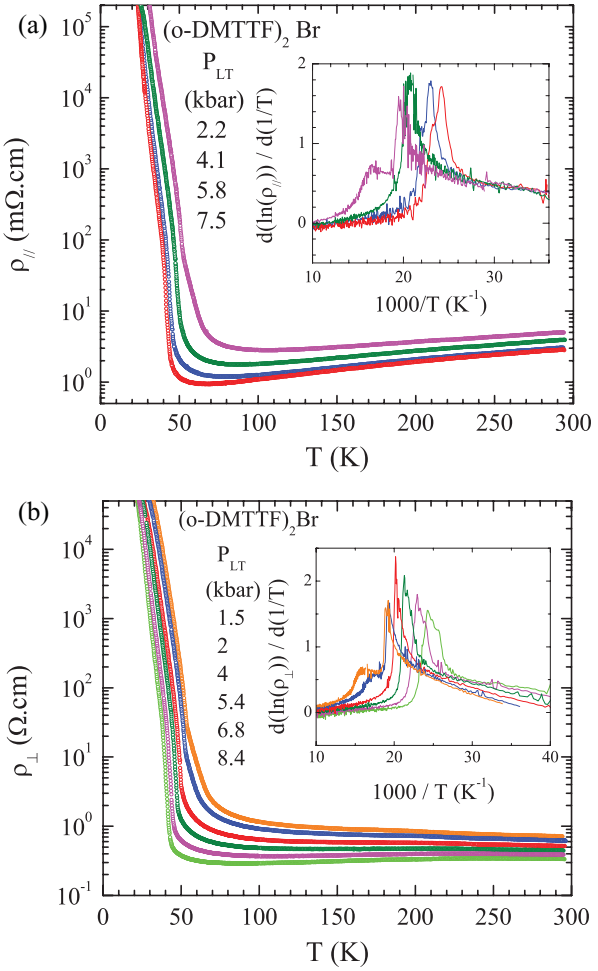

FIG. 4. (Color online) Evolution of the longitudinal (a) and transverse (b) resistivity versus temperature in (o-DMTTF)$_2$Br for different pressures. Each figure shows successive applied pressure on the same sample. Inserts: d(ln(ρ))/d(1/T) as a function of temperature for all pressures. The characteristic temperatures T_c and T_u of Fig. 16 correspond to the positions of the right and left (if it exists) peaks, respectively.

temperature for T^*. Below T^*, the transverse resistivity follows a metallic behavior down to about 80 K, where a weak increase of the resistivity is observed.

Transverse resistivity, $\rho_\perp$, measurements under pressure have also been performed on the Br salt [Fig. 4(b)] and lead to the same conclusion for the pressure dependence of T_u and T_c. Below 5 kbar, $\rho_\perp$ exhibits a localization behavior at all temperatures. Above 5 kbar, a weak maximum of the resistivity occurs between 200 and 300 K at a temperature denoted T^* whose value increases with pressure. This temperature cannot be associated with the solidification of the pressure medium, which is also visible as a small bump on both longitudinal and transverse resistivity curves between 170 and 250 K at a temperature also increasing with pressure. Below T^*, the transverse resistivity follows a metallic behavior down to about 70–80 K, where a weak increase of the resistivity is observed.

The differential longitudinal conductance has been measured in (o-DMTTF)$_2$Br at low temperature for all pressures shown in Fig. 4(a). The data are shown only for the two lowest pressures [see Fig. 5]. Nonlinearities are clearly visible, and a threshold field of about 150 mV/cm at P = 2.2 kbar and 100 mV/cm at P = 4.1 kbar can be extracted at T = 21 K. These nonlinearities disappear upon increasing the temperature and are no more visible above T_c. This threshold field also decreases smoothly upon increasing pressure.

In the I salt, as shown in Fig. 6, although the metallic regime is well established at high temperature, the resistivity data do not present any clear accident below T_ρ in particular around 50 K at variance with the Cl and Br salts. This is well illustrated in the $d(\ln(\rho))/d(1/T)$ versus 1/T curves shown in the insert of Fig. 6.

From the temperature dependence of the transverse and longitudinal resistivities measured on the Cl and Br salts below T_c, an activation energy, E_a, can be extracted. However, no saturation is observed at low temperature in the $d(\ln(\rho))/d(1/T)$ versus 1/T plots. Therefore, we will define the charge gap at ambient pressure, as twice the activation energy $\Delta\rho$ measured around 30 K. From transverse resistivity data, we get a charge

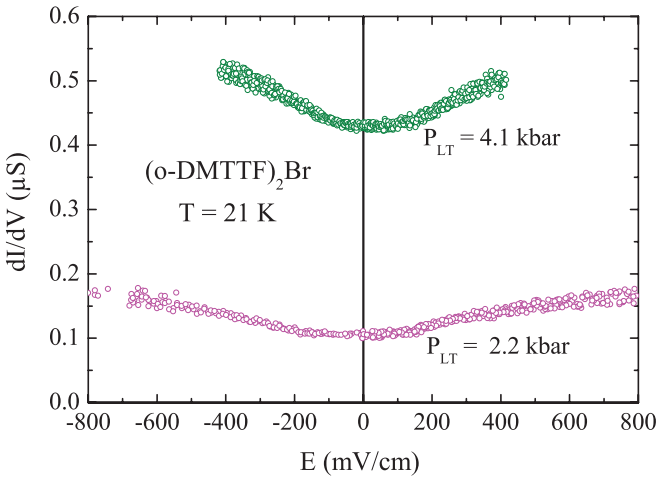

FIG. 5. (Color online) Longitudinal differential conductance versus the applied electric field in (o-DMTTF)$_2$Br at 21 K for the two first pressures shown in Fig. 4(a).

gap of about 600 and 640 K for Cl and Br salts, respectively. From longitudinal resistivity data, similar values are obtained at low pressure, as long as T_c is close to 50 K. When T_c decreases, the activation energy has to be evaluated at lower temperature in order to be far enough from the peak detected in $d(\ln(\rho))/d(1/T)$ versus 1/T plots (inserts of Figs. 3 and 4). Consequently, we cannot give the precise evolution of the charge gap with pressure from resistivity data measured down to 20 K. In the I salt, despite the transition not being well defined, a charge gap can be extracted at low temperature, which evolves from 800 K at 8 kbar down to 340 K at 18 kbar.

In order to get more information about this phase diagram, we performed thermopower measurements. The Seebeck coefficient, S, along the c-axis has been measured at ambient pressure for all three salts. At room temperature, its value of 15 μV/K is similar to other observations in organic conductors.[55] As shown in Fig. 7, S varies linearly with

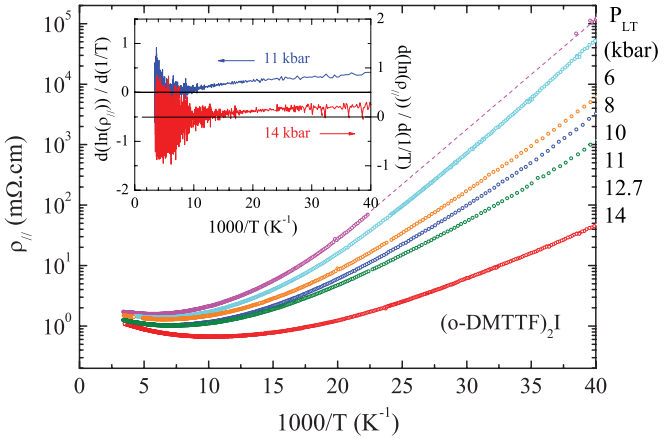

FIG. 6. (Color online) Evolution of the longitudinal resistivity versus the inverse of the temperature for different pressures in (o-DMTTF)$_2$I. Insert: d(ln(ρ))/d(1/T) as a function of temperature at 11 and 14 kbar showing the absence of any clear maximum around 50 K.

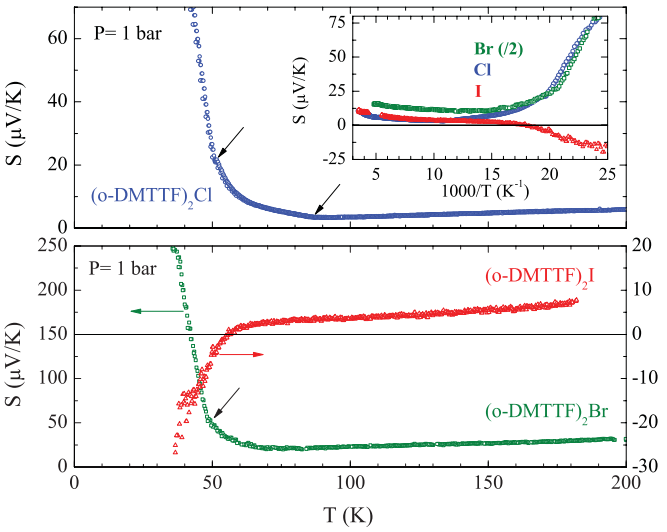

FIG. 7. (Color online) Evolution of the Seebeck coefficient, S, as a function of temperature at ambient pressure in the (o-DMTTF)$_2X$ series. The black arrows indicate characteristic temperatures T_c and T_u plotted as diamonds in Fig. 16. Insert: S versus 1/T in all three compounds. In (o-DMTTF)$_2$Br, the value of S has been divided by 2 for clarity and a better comparison.

temperature even below T_ρ for all compounds. The metal-insulator transition manifests itself by a change of slope with a deviation toward positive values for the Cl and Br salts and negative values for the I salt. Such deviations in various directions are well-known in the (TMTTF)$_2X$ series.[56] In the Cl salt, two breaks appear clearly at 80 and 50 K in agreement with the resistivity measurements. In the Br salt, the transition appears to be smoother with a deviation from the "metallic" behavior around 60 K and a steepest increase at 49 K, which again mimics the resistivity behavior. Finally, in the I salt a unique smooth transition occurs at about 60 K.

From the linear part in the metallic regime and considering the thermopower derived for a metallic system and a three-quarter-filled band,[57] $S = \frac{2\sqrt{2}}{3}\pi^2 \frac{k_B}{e}\frac{k_B T}{W}$ where W is the bandwidth, we obtain W $\approx$ 1.4 eV, so a longitudinal transfer integral of about 0.35 eV in fair agreement with band structure calculations for all three compounds.[51] In the insulating state, the insert of Fig. 7 shows that S varies linearly with 1/T, as expected for an insulator from which we can deduce the gaps Δ_{TEP} = 260, 365, and 33 K for the Cl, Br, and I salts, respectively. Δ_{TEP} is much smaller than the charge gap measured by resistivity similarly to other molecular compounds.[56] We attribute the small values of Δ_{TEP} to impurity levels in the semiconducting gap.

IV. MAGNETIC MEASUREMENTS

Let us first describe the ESR data. As specified in the experimental part, this study has been performed on oriented single crystals, and the measurements as a function of the temperature have been realized along the principal magnetic axes.

For convenience, we shall begin with the description of data obtained from the Cl salt and later compare them with the results obtained for the two other salts. For any direction

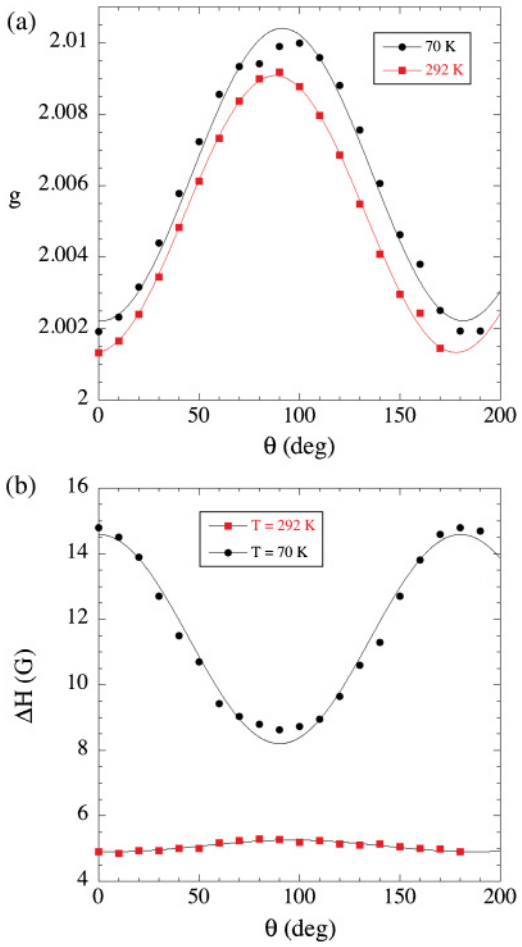

FIG. 8. (Color online) (a) Rotation pattern for the g factor at room temperature and 70 K for (o-DMTTF)$_2$Cl at ambient pressure. (b) Rotation pattern for the linewidth at room temperature and 70 K for (o-DMTTF)$_2$Cl at ambient pressure.

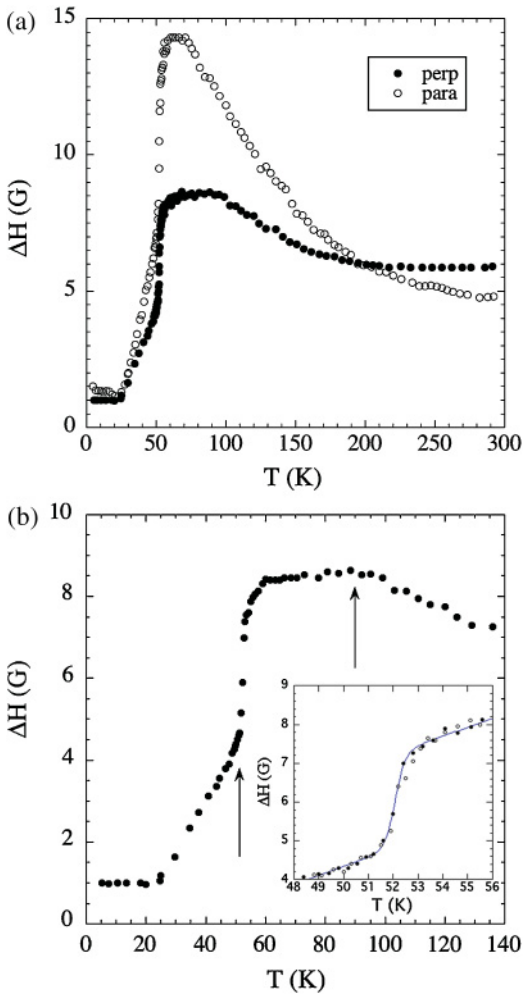

FIG. 9. (a) Temperature dependence of the ESR linewidth along the two principal magnetic directions of (o-DMTTF)$_2$Cl at ambient pressure. (b) Zoom of the temperature dependence of the ESR linewidth of (o-DMTTF)$_2$Cl at ambient pressure along the perpendicular direction. The arrows show the expected location of the two phase transitions described in the text. Details close to 52 K are shown in the inset.

of the applied magnetic field, a single ESR line is observed. Most of the time, a Lorentzian shape was found, but in some cases Dysonian (asymmetric) lines have been also observed as described later. As mentioned in the experimental part, extrema of the g factor and linewidth were found along the chain axis and perpendicularly to it. This point is emphasized on Figs. 8(a) and 8(b), which report the observed rotation patterns. In these two figures, the origin of the angle θ is taken when the magnetic field is applied along the chain axis. Then, for $\theta = 90^\circ$ the field is applied in the (**a**, **b**) plane, where an isotropic signal was found at any temperature within the experimental accuracy. Along the chain axis, the g factor is close to the free-electron value (2.0023) in consistence with the fact that the field is then applied perpendicularly to the molecule axis. The maximum in the perpendicular orientation is close to 2.009. Both values are only weakly temperature dependent. Although the linewidth rotation patterns show a standard sinusoidal shape, two regimes of relaxation are emphasized by the observation that the position of the maximum shifts from $\theta = 90^\circ$ to $\theta = 0^\circ$ as the temperature decreases [Fig. 8(b)]. This crossover is also visible around 200 K in Fig. 9(a), which compares the temperature dependences of the linewidth along the two principal magnetic directions.

In most organic salts composed of only one type of chain (like (TMTT(S)F)$_2X$ salts), the ESR linewidth is a decreasing function of the temperature. This behavior has been explained in the TMTSF series evoking symmetry arguments, strictly valid at zero temperature, which explains that the linewidth increases when torsional oscillations are activated by raising the temperature.[58] The situation is different in "two chains compounds" like TTF-TCNQ when the single observed ESR line results of a hybridation between the two kinds of chains. In this latter case, the temperature dependence of the ESR linewidth mimics the one found for the electrical conductivity[59] (for a review about ESR in organic conductors, see, for example, Ref. 60). The (o-DMTTF)$_2X$ materials should in fact be described as two chains compounds because two distinct chain orientations are present in the crystal structure (see Fig. 1). One may then argue that the data shown in the Fig. 9 mimics the conductivity temperature dependence given in Figs. 2 and 3 as it was the case in TTF-TCNQ. However, a detailed quantitative theory of the

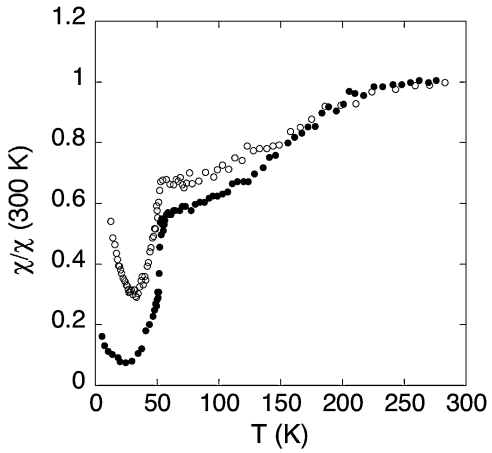

FIG. 10. Temperature dependence of the spin susceptibility deduced from ESR for $(o\text{-DMTTF})_2Cl$ (black dots) and $(o\text{-DMTTF})_2Br$ (open dots) at ambient pressure. The data have been normalized at room temperature.

ESR linewidth in such anisotropic systems is still missing to deepen this discussion. It is however interesting to notice that when decreasing the temperature, two slight anomalies are found in the linewidth thermal dependence [Fig. 9(b)]: first, a sharp decrease occurs at 52 K. Nevertheless, no evidence for a hysteresis was found [see inset of Fig. 9(b)]. This corresponds to the location of the phase transition found with the other experimental techniques. Moreover, one may observe a change of slope around 80–90 K but only in the perpendicular direction. This may be eventually associated with the anomaly observed around 80 K with conductivity measurements (see the above discussion) but taken alone, this experimental result cannot be taken as a proof for a phase transition. Finally, the spin susceptibility deduced from the double integration of the ESR signal is shown in Fig. 10 (black dots). A drop of the spin susceptibility occurs at 52 K, indicating a diamagnetic low-temperature ground state. Note that a small Curie component is present below 20 K.

Let us now compare the ESR data obtained with the Br and I salts. As in the previous case, extrema of the g factor and linewidth were obtained along the parallel and perpendicular directions. Because of the broader linewidth, the determination of the g factor becomes much less accurate. However, values essentially consistent with the one deduced for the Cl salt were found, and we shall essentially discuss the temperature dependence of the linewidth and spin susceptibility. The temperature dependence of the linewidth in the two principal magnetic directions of the Br salt was already shown in Fig. 5 of Ref. 51. With respect to the data of the Cl salt, both kinds of linewidths of the Br salt are larger, and the minimum value is always found along the perpendicular direction: in this case if a crossover exists, it should be located above 300 K. Low-temperature data for the transverse direction are shown in Fig. 11(a). There is still a clear phase transition around 50 K, although the decrease of the linewidth is not as sharp as for the Cl salt. Finally, a maximum of the linewidth in the transverse direction is found around 70 K, comforting the occurrence of a phase transition around this temperature as deduced from transport measurements. The spin susceptibility of the Br salt

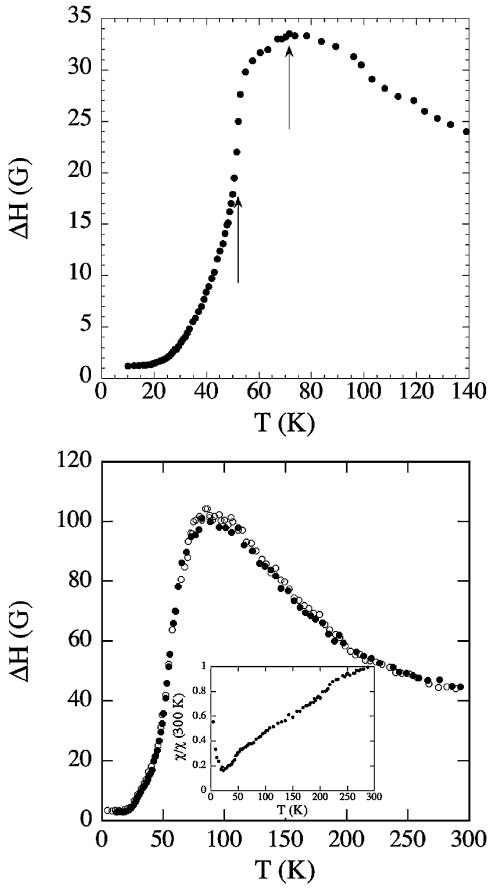

FIG. 11. (a) Temperature dependence of the ESR linewidth of $(o\text{-DMTTF})_2Br$ at ambient pressure when the magnetic field is applied along the perpendicular direction. The arrows show the expected location of the two phase transitions described in the text. (b) Temperature dependence of the ESR linewidth along the two principal magnetic directions for $(o\text{-DMTTF})_2I$ at ambient pressure [same symbols as Fig. 9(a)]. The corresponding spin susceptibility is shown in the inset.

is compared with the one for the Cl salt in Fig. 10 (open dots). The striking difference is a much larger Curie component for the Br salt. As previously mentioned,[51] this extrinsic signal quickly becomes the dominant contribution to the ESR signal below 50 K. In this context, the shift of the g factor previously reported (Fig. 6 in Ref. 51) is probably extrinsic. In fact, this g factor shift is not observed for the Cl salt, and it depends on the sample batch for the Br salt. Figure 11(b) shows the temperature dependence of the linewidth for the I salt. In this case, the ESR signal becomes very broad and an accurate determination of the ESR data is difficult at high temperature. Within experimental errors, the anisotropy of the linewidth is negligible. However, thermal variations are consistent with the one of the other salts of the series. A drop of the linewidth around 50 K indicates the occurrence of a phase transition. However, this anomaly is now ill defined as emphasized by the spin susceptibility shown in the inset of Fig. 11(b). In particular, the low-temperature Curie component becomes very large for this salt.

Let us now discuss how ESR data can allow getting information on the electrical conductivity. In a previous work, three

of us have shown that the asymmetry of the ESR line (usually noted A/B) can be used to deduce quantitative information on the electrical conductivity tensor.[61] More precisely, for a given orientation of the crystal, this technique probes the two components of the conductivity tensor located in the plane perpendicular to the microwave magnetic field. The analysis of experimental data is facilitated when the measured asymmetry is used to deduce the parameter α that can be theoretically calculated as a function of the sample dimensions and components of the conductivity tensor. The most complete study has been performed on a big Br single crystal (typical dimensions $0.3*0.5*1.6$ mm^3) for which the ESR line was found to be asymmetric for both orientations of the crystal. One of them directly probes the plane perpendicular to the chain axis. We found $\alpha \approx 0.05$ at room temperature. For this small value of the asymmetry, the approximate expression: $\alpha \approx \lambda^2/3$ can be used, where λ is the ratio between the sample dimension and the skin depth in the probed direction. In this limit, α is directly proportional to the transverse conductivity. The values of the transverse resistivity thus deduced are plotted in function of the temperature in Fig. 12(a). In the other orientation, where the microwave magnetic field is perpendicular to the chain axis, one probes the (**a**, **b**) plane. The general expression of α for a rectangular crystal section is given in Ref. 61. Introducing numbers in this expression shows that $\alpha \approx {\lambda_x}^2/3$ is a good approximation, where $\lambda_x = l/d_{\mathrm{perp}}$ (l is the sample dimension along the chain axis, and d_{perp} is the skin depth in the transverse direction). The consequence is that this orientation also probes the transverse conductivity. In fact, the deduced values of the resistivity also shown in Fig. 12(a) are consistent with the one obtained in the first orientation. Although the absolute values are only smaller by a factor of two than the one found from dc measurements (Fig. 2), a similar temperature dependence is found and an electronic localization is clearly visible below 80 K.

Many attempts were made in order to obtain results with thinner samples (to deduce information on the parallel conductivity), but thin samples are more brittle, and cracks occur during thermal cycling of the samples. Moreover, for these thinner crystals, only the orientation which probes the (**a**, **b**) plane gives a measurable asymmetry. For these two reasons, the determination of absolute values of the resistivity becomes impossible. Finally, iodide samples were so brittle that we shall essentially present our best result for the chlorine salt. Figure 12(b) gives the temperature dependence of $1/\alpha$ normalized at room temperature. In this case, a metallic regime is visible at high temperature, suggesting that an important contribution of the longitudinal conductivity enters in the result. A clear, activated regime (with an activation energy Δ_ρ of about 550 K) is seen below 80 K consistent with dc conductivity data.

To complement the ESR experiment, SQUID measurements have been performed with polycrystalline samples. Figure 13(a) shows the magnetic susceptibility obtained after subtraction of the sample holder at 10 000 Oe. At this field, the contribution of ferromagnetic impurities becomes very small and can be neglected. The 50-K phase transition is clearly observed. Moreover, a Curie component is always seen at low temperature. It corresponds to typically 0,2% of $S = \frac{1}{2}$ magnetic defects per DMTTF mole, i.e., to a very

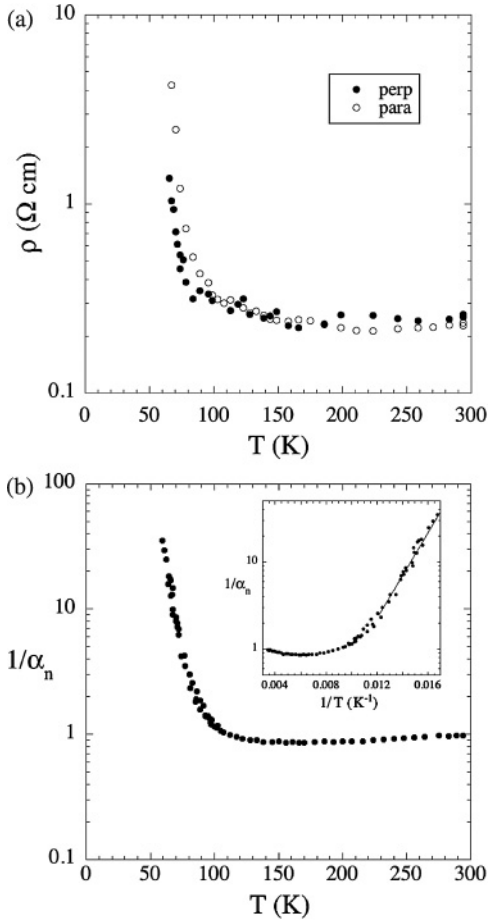

FIG. 12. (a) Temperature dependence of the transverse resistivity deduced from ESR data along the two principal magnetic directions for (o-DMTTF)$_2$Br at ambient pressure. (b) Temperature dependence of $1/\alpha$ normalized at room temperature, deduced from ESR data for (o-DMTTF)$_2$Cl at ambient pressure. In the inset, the same data plotted as a function of $1/T$ demonstrates the activated regime below 80 K.

small amount of defects. Note that, at least for the Cl salt, the amount of defects is significantly larger on the powder sample than on the single crystal measured by ESR. This confirms the extrinsic origin of these defects. To support this analysis, magnetization has also been measured at low temperature as a function of the applied field. The inset of Fig. 13(a) shows the result obtained for the Cl salt at 1.9 K. An excellent fit is obtained with the Brillouin function for $S = \frac{1}{2}$ spin (continuous line in this figure). Similar data were obtained for the other salts. The minimum value should be of the order of the core diamagnetism calculated from the Pascal constants. Strictly speaking, one should obtain -2.5×10^{-4}, -2.7×10^{-4}, and -3×10^{-4} for the Cl, Br, and I salts, respectively in electromagnetic units (emu). Experimentally, slightly smaller values are found that may be explained by the limited accuracy when the diamagnetic component for the sample holder is removed (the sample mass and therefore the sample signal is very small). Thus, we decided to assume a perfect diamagnetic ground state at low temperature and thus to subtract a contribution of the form $C/T + A$ to the experimental susceptibility (C and A being obtained by a fit

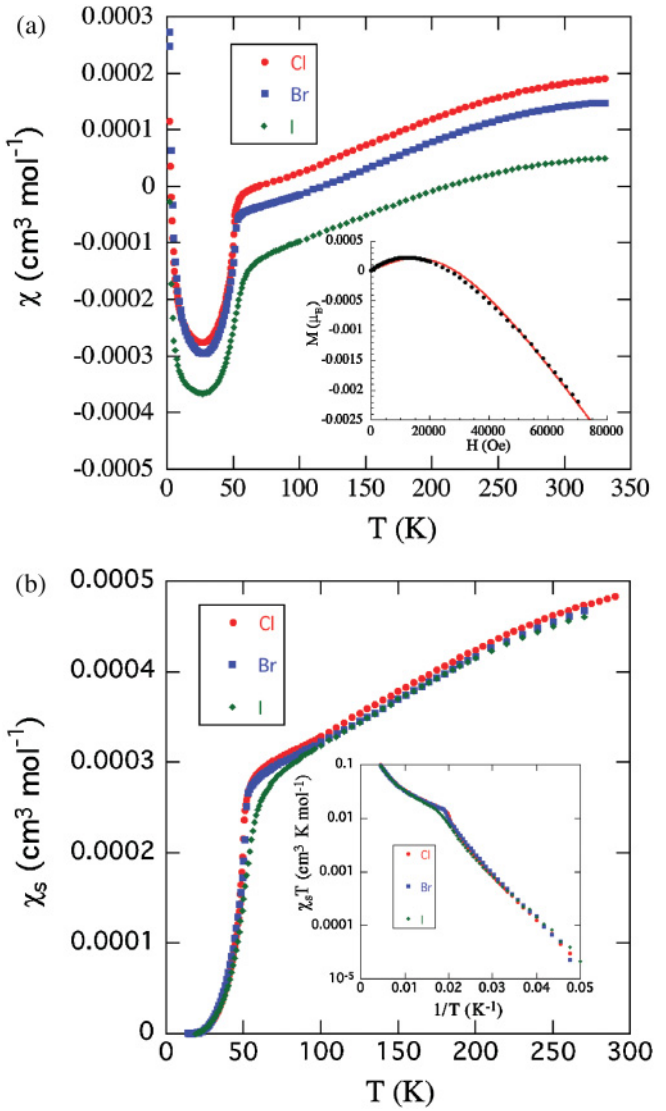

FIG. 13. (Color online) (a) Temperature dependence of SQUID magnetic susceptibility (measured at 10 000 Oe for the three salts at ambient pressure. In the inset, field dependence of the magnetization at 1.9 K for the Cl salt. The continuous line gives the fit to a Brillouin function for $S = \frac{1}{2}$. (b) Temperature dependence of spin susceptibility for the three salts at ambient pressure as deduced from the SQUID measurement. In the inset, semilog plot of $\chi_S T$ versus $1/T$ to emphasize the low-temperature activated behavior.

of the magnetic susceptibility below typically 20 K). The remaining component, identified as the spin susceptibility, χ_s, is shown in Fig. 13(b). As expected, very similar spin susceptibility values are obtained in the high-temperature paramagnetic phase. The absolute value obtained (of the order of 5×10^{-4} cm^3/mol at room temperature) is significantly larger than the expected Pauli susceptibility and therefore supports the existence of electronic correlations. Moreover, the T_c phase transition appears to be sharper for the Cl or Br salts than for the iodide salt. An activated behavior is found below this phase transition as emphasized by plotting $\ln(\chi_S T)$ versus $1/T$ [see inset of Fig. 13(b)]. A similar activation energy Δ_σ of about 190 K is found for the three compounds. All these data are consistent with transport measurements results.

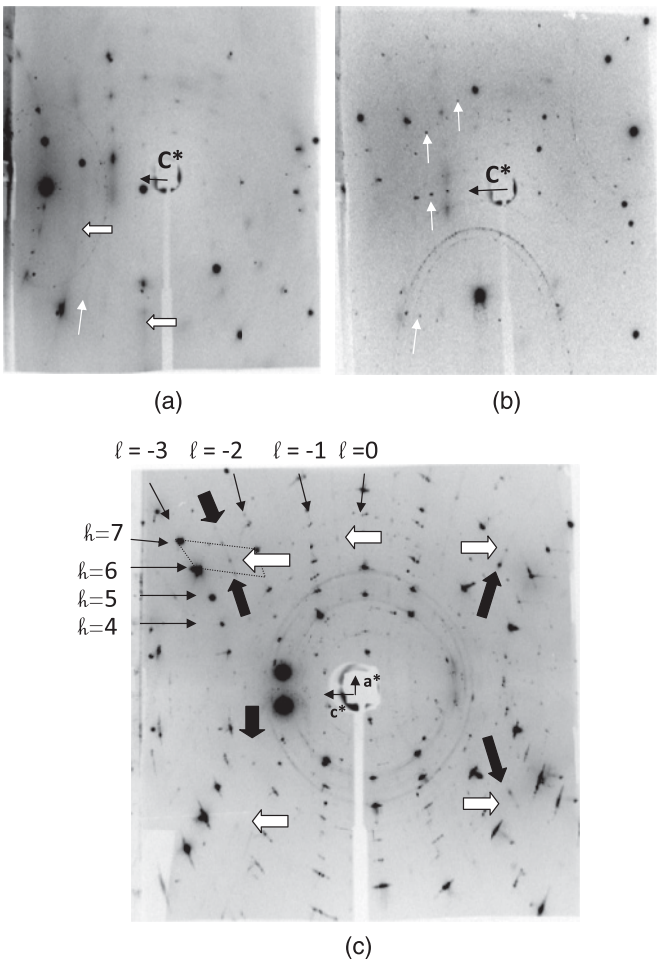

FIG. 14. X-ray pattern of (o-DMTTF)$_2$Br at ambient pressure taken at 70 K (a) and 35 K (b). In (a) and (b), the c^* axis is indicated by black arrows, while the $2k_F$ diffuse lines and satellite reflections are shown by small white arrows, and $4k_F$ diffuse lines are represented by big white arrows. (c) X-ray pattern of (o-DMTTF)$_2$I at ambient pressure taken at 40 K. In (c) the h and l integer Bragg layers are indicated by thin black arrows. A unit cell is represented by dotted lines. The $q_c = (1/2,?,1/2)$ and $q_c = (0,?,1/2)$ sets of satellite reflections are shown by thick white and black arrows, respectively.

V. X-RAY DIFFUSE SCATTERING MEASUREMENTS

In order to get information on the structure of the insulating state, a qualitative investigation of the diffuse scattering has been performed on the three salts at ambient pressure using the photographic method. Weak diffuse lines appear below about $T_{fl} = 75 \pm 10$ K for the Cl salt and $T_{fl} = 100 \pm 20$ K for both the Br and I salts. The x-ray patterns taken at T = 70 K show that the weak diffuse lines are observed only for large diffraction angles and are absent along the c^* direction [Fig. 14(a)]. These diffuse lines are perpendicular to the c direction and located halfway between successive $\mathbb{I}$ integer Bragg layers. They correspond to the intersection of the Ewald sphere with diffuse sheets perpendicular to the c-axis in the reciprocal space. In direct space, this corresponds to 1D pretransitional structural fluctuations with the critical wave vector $q_c = 1/2$ c^*, correlated along the chain direction but decoupled between neighbor chains. Indeed, the full width at half maximum of

the diffuse lines (corrected of the experimental resolution and using the convention $cc^* = 2\pi$) is 0.06 $Å^{-1}$ for the Br and I salts at 70 K. For the Cl salt, the measurement was not possible because of the weakness of the diffuse scattering. This corresponds to a quite large correlation length of about eight intermolecular distances along the chain axis. It should be noticed also that the intensity of the diffuse lines is of the same order of magnitude for both compounds Br and I. As the intensity is proportional to the square of the structure factor, $F(\vec{Q})$ of the entity undergoing the pretransitional fluctuations, we can conclude that the 1D fluctuations basically concern the molecular stack for the Br and I salts. Furthermore, the observation of diffuse lines at large diffraction angles indicates that the structural instability is due to a displacive effect. Assuming a rigid molecular displacement $\vec{u}$, the diffuse intensity is given by $I(\vec{Q}) \propto |F(\vec{Q})|^{2*}(\vec{Q}.\vec{u})^2$. The absence of diffuse lines along the $c = c^*$ direction (i.e., when $\vec{Q}//c^*$), allows us to conclude that the polarization of the displacement $\vec{u}$ is perpendicular to c. The finding of a displacement aligned in the molecular plane is a common feature in molecular conductors because this polarization leads to a large electron-phonon coupling (large variation of the transfer integral for a low cost of elastic energy). In particular, in order to achieve a first-order electron-phonon coupling, the polarization must be located in the symmetry plane of the stack.[62] In the present case of a zigzag arrangement and for a polarization perpendicular to c, the displacement should be directed along the long axis of the molecule.

It is important to notice that additional thin and weak diffuse segments are observed above T_u on the x-ray pattern of the Br and Cl salts inside the Bragg layers perpendicular to c^*. The origin of this x-ray scattering can be attributed to $4k_F = c^*$ pretransitionnal fluctuations. In the I salt, this diffuse scattering is not observed.

The x-ray diffuse scattering investigation of the Cl salt does not reveal any important structural modification below $T_u = 80$ K. However, the sample used was not of good enough quality to rule out a structural modification breaking some symmetry elements of the high-temperature $I\bar{4}2d$ space group as the result of the condensation of the $4k_F$ diffuse lines.

Upon cooling below $T_c \approx 50 \pm 2$ K for the Cl and Br salts and $T_c \approx 48 \pm 2$ K for the I salt, the $\frac{1}{2}$ c^* diffuse lines condense into q_c satellite reflections having the experimental resolution [see Figs. 14(b) and 14(c)], indicating the occurrence of a 3D long-range structural transition. The relative intensity of the satellite reflections with respect to the mean Bragg reflections (I_{sat}/I_{Bragg}) is about 10^{-2} for the Cl and Br salts and 2.10^{-2} for the I salt. The increase of the ratio I_{sat}/I_{Bragg} from Cl, Br to I shows that the anions must contribute to the scattered intensity of the satellite reflections and thus participate to the 3D modulation pattern stabilized below T_c. In addition, the important values of the scattered intensities of the satellite reflections show that the structural effect is strong compared to those observed for the Peierls transition in other molecular conductors such as TTF-TCNQ, where the $2k_F$ superstructure reflections are 7.10^{-4} less intense than the mean Bragg reflections.[63] This leads to an amplitude for the atomic displacements, which is four times stronger in the (o-DMTTF)$_2X$ compounds than in TTF-TCNQ, while the ratio of the charge gaps is only of two. The difference between the charge gap (related to the molecular stack) and the amplitude of the atomic displacements indicates that not only the molecular stack is involved in the lattice distortion but also the anions. This thus confirms that the anions play part of the 3D modulation, as observed for instance in the anion ordering of $(TMTSF)_2ReO_4$.[31]

Let us now come back to the q_c reflections observed below T_c. The component of the satellite reflections along the c^* direction is 1/2. This means that the Bravais lattice is doubled along the c direction below T_c. This doubling is certainly due to a tetramerization of the zigzag stack. In these 2:1 salts, the conduction band associated with the uniform molecular stack with a periodicity c′, is three-quarter filled, leading to a $2k_F = 1/4c'^*$ critical wave vector. However, the real crystallographic periodicity is $c = 2c'$, and thus in the crystallographic folded Brillouin zone, one has $2k_F = 1/2c^*$. This accounts for the wave vector component experimentally observed in all the salts.

The indexation of transverse (a*, b*) components of the satellite reflections that have been performed via the inspection of x-ray patterns is difficult. The difficulty is due first to the large value of the tetragonal a = b lattice parameters and second to the fact that one of the reciprocal directions is systematically missing on the x-ray pattern, which is a 2D projection of the reciprocal space. In our case, the x-ray patterns correspond to the projection of (c^*, a*) planes (or to the symmetry equivalent (c^*, b*) planes assuming that the tetragonal symmetry is kept). In the x-ray patterns taken from Cl, Br, and I salts, we have systematically observed two types of satellite reflections. The first type of satellite reflections [shown by big black arrows in Fig. 14(c)] were located half way between two successive h integer Bragg layers. In that case, the reduced critical wave vector is $q_c = (1/2,?,\pm 1/2)$ (or the symmetry equivalent $q_c = (?,1/2, \pm 1/2)$ where a and b are interchanged). The second type of satellite reflections [shown by big white arrows in Fig. 14(c) were located exactly on the h integer Bragg layers, which lead to $q_c = (0,?, \pm 1/2)$ [or the symmetry equivalent $q_c = (?,0, \pm 1/2)$]. Both indexations are compatible only if the critical wave vectors of the structural modulation are (1/2, 0, ±1/2) and (0, 1/2, ±1/2). At the present stage of our investigation we do not know if the satellites belong to the same domain of modulation or belong to different domains. It should be remarked that for the $I\bar{4}2d$ space group, the critical wave vectors inside the sets {(1/2, 0, 1/2), (1/2, 0, −1/2)} or {(0, 1/2, 1/2), and (0, 1/2, −1/2)} are not equivalent because they do not differ by a reciprocal wave vector of the I centered reciprocal lattice.

A quantitative study of the thermal dependence of the intensity of the satellite reflections has been performed using the lifting 1D gas detector. The measurement has been performed for several satellite reflections of the Cl, Br, and I salts upon heating. The measurements show that the profile of the satellite reflections is not modified until T_c is reached. In these conditions, the peak intensity of the satellite reflections is proportional to the integrated intensity, which is itself proportional to the square of the order parameter of the structural transition. The Fig. 15 presents for the three salts, the peak intensity, I(T), of one satellite reflection divided by the peak intensity I_0 at T = 10 K, $I(T)/I_0$, as a function of the reduced temperature T/T_c. In the Cl salt, the experimental

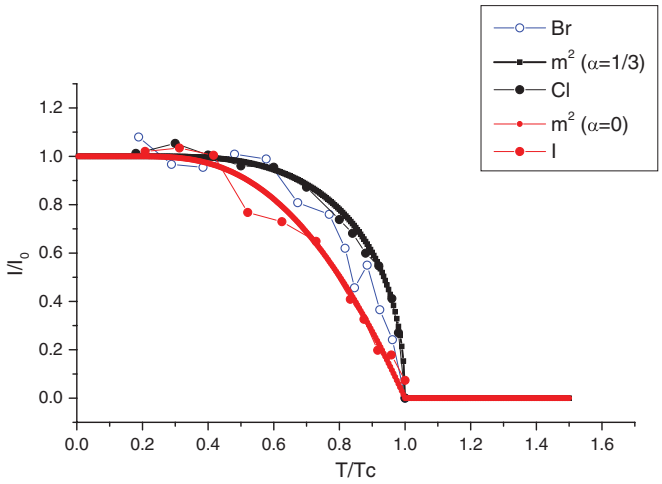

FIG. 15. (Color online) (a) Variation of the peak intensity I(T) divided by the intensity I_0 at 10 K, $I(T)/I_0$, as a function of T/T_c for the Cl, Br, and I salts at ambient pressure. This figure gives also the thermal dependence of the square of the mean-field order parameter m(T) calculated for a second-order transition ($\alpha = 0$) and a tricritical point ($\alpha = 1/3$) (red/dark gray and black continuous lines, respectively).

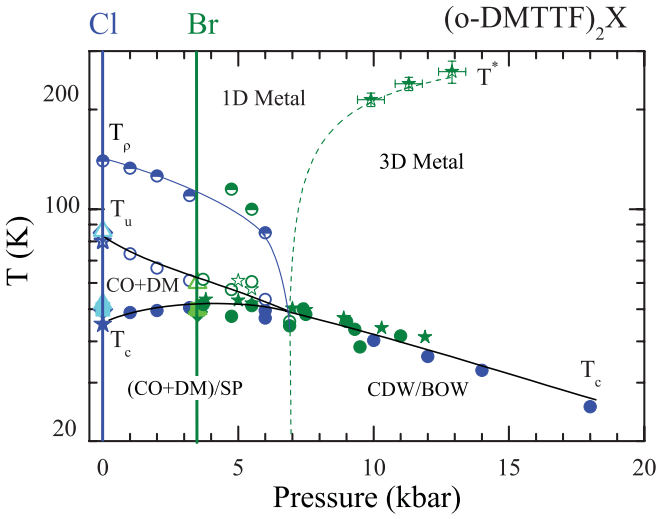

FIG. 16. (Color online) Generic pressure-temperature phase diagram of the $(o\text{-DMTTF})_2X$ series. The origin of pressure is taken for the Cl salt (blue symbols), and data for the Br salt (green symbols) are shifted by 3.5 kbar. Closed symbols indicate the temperature T_c, open symbols, T_u and half-filled symbols, T_ρ (minimum of the longitudinal resistivity), and T^* (maximum of the transverse resistivity). Data points plotted as circles (stars) are extracted from longitudinal (transverse) resistivity measurements for different applied pressures and different samples. At ambient pressure, data points plotted as diamonds, triangles, and squares are deduced from TEP, ESR, and x-ray measurements, respectively. Lines are guides to the eye.

points shown correspond to the measurement of a unique satellite reflection of strong intensity. For the Br and I salt, in order to improve the statistic, the experimental points shown correspond to the average of the data obtained for two different satellite reflections. For comparison, the Fig. 15 also gives the thermal dependence of the square of the mean-field order parameter m(T) for a second-order transition ($\alpha = 0$) and a tricritical point ($\alpha = 1/3$) according to a phenomenological free-energy calculation detailed in Ref. 64.

Figure 15 shows that the thermal dependence of $I(T)/I_0$ is quite different for the three salts. In the Cl salt, there is a quite abrupt decrease of intensity near T_c. The decrease is much smoother for the I salt. The behavior of the Br salt is intermediate between those of the Cl and I salts. This interesting behavior will be discussed in the following section.

VI. DISCUSSION

The experimental data shown here above allow us to propose a tentative (pressure, temperature) phase diagram of the $(o\text{-DMTTF})_2X$ family. We first discuss the high-temperature precursor (fluctuations) properties, then the ground states and the phase diagram. We discuss both the Cl and Br compounds, which could be placed on a universal phase diagram with a pressure shift of 3.5 kbar (Fig. 16). The case of the I salt, which is more complicated, will be discussed separately.

A. Pretransitional effects

We first discuss the high-temperature region above the different ground states, especially the fluctuation effects. For all three compounds of the family, both transport and ESR measurements demonstrate that the system is metallic at room temperature and ambient pressure with a strong anisotropy of resistivity in agreement with the band calculations.[51] At room temperature, the spin susceptibility, χ_s, far exceeds its standard Pauli value, which suggests an important role of the electronic correlations. Upon cooling below T_ρ, a weak electronic localization is observed on the resistivity and the ESR linewidth curves associated with a decrease of the spin susceptibility.

From the low-temperature value of the charge gap $2\Delta_\rho$, we may determine a mean-field temperature from the Bardeen Cooper Schrieffer (BCS) relationship $2\Delta_\rho = 3.56 k_B T_\rho^{MF}$. One obtains $T_\rho^{MF} \sim 225$ K, which must be the onset temperature of the charge fluctuations. At about this temperature, there are thermal changes in the Raman and infrared spectra.[65] Surprisingly T_ρ^{MF} is significantly larger than both the localization temperature T_ρ shown in Fig. 16 and the temperature T_{fl} at which the $2k_F$ fluctuations begin to be detected.

As in the Cl salt, T_ρ is much larger than T_{fl}, so that the electron localization cannot be related to electron-phonon interactions inducing a pseudogap in the electronic degrees of freedom. This is a general trend observed in $(TMTTF)_2PF_6$, where T_{fl} is smaller than T_ρ.[66] We believe that this localization is related to electron-electron correlations inducing $4k_F$ fluctuations. The diffuse lines observed in the x-ray patterns of the Br and Cl salts [see Fig. 14(a)] can be the fingerprint of these $4k_F$ fluctuations. High-temperature 1D $4k_F$ fluctuations are commonly observed in quarter-filled organic salts based on the TCNQ or DCNQI acceptor derivatives, such as $Qn(TCNQ)_2$,[67] $(DMe\text{-}DCNQI)_2Ag$,[41] and $(DI\text{-}DCNQI)_2Ag$,[43]

or on the TTF or TSF donor derivatives, such as TMTTF-DMTCNQ and TMTSF-DMTCNQ,[62] the only exception being the $(TMTTF)_2X$ series.[68] These $4k_F$ fluctuations are also systematically observed when the band filling is very close to one-quarter, such as in $(TMTTF)_2$ Bromanil,[69] DBTTF-$TCNQCl_2$,[70] BTDMTTF-TCNQ,[71], and the solid solution $(NMP)_x(Phen)_{1-x}$ TCNQ for $x \sim 0.5$.[72] In TMTSF-DMTCNQ and BTDMTTF-TCNQ the high-temperature $4k_F$ fluctuations vanish upon cooling, but in the other salts they condense either into a high-temperature $4k_F$ modulation or give rise to a $4k_F$ short-range order in the presence of disorder. The 1D $4k_F$ x-ray diffuse scattering detected in the above-quoted organic salts more likely corresponds to a $4k_F$ BOW or DM structural instability originating from the coupling of acoustic phonons with the $4k_F$ electronic instability.[62] The nonobservation of such a scattering in the $(TMTTF)_2X$ could be easily understood because the $4k_F$ BOW instability is probably killed by the presence of the incipient dimerization of the stack. The remaining $4k_F$ CO instability is more difficult to detect because it involves internal deformations modes of the molecule. In addition such an instability could have a 3D anisotropy if it is coupled to the anion sublattice (as for the AO transitions in the $(TMTTF)_2X$ and $(TMTSF)_2X$[31,68]). In addition, with a CO transition in $(TMTTF)_2X$ keeping the translation symmetry, such 3D $4k_F$ fluctuations should be centered on the Bragg reflection positions, which renders their detection very difficult by photographic techniques. The observation of 1D $4k_F$ fluctuations in $(o\text{-DMTTF})_2Cl$ and Br by these techniques should more likely correspond to the detection of the DM counterpart of the $4k_F$ lattice instability involved in the T_u transition (see next section).

In parallel with the decrease of T_ρ from the Cl to the Br salt, one observes an increase of T_{fl}, which means an enhancement of the $2k_F$ BOW fluctuations. In the Br salt T_{fl} occurs at about T_ρ. A similar feature was previously noticed along the $(TMTTF)_2X$-$(TMTSF)_2X$ sequence[66] and especially when x decreases in the $[(TMTSF)_{1-x}\ (TMTTF)_x]_2ClO_4$ solid solution.[73,74]

B. The upper transition at T_u

In the low-pressure range of the Cl and Br salts, two distinct anomalies are revealed by conductivity and thermopower measurements. At ambient pressure the upper anomaly, T_u, occurs at about 80 and 60 K for the Cl and Br salts, respectively, i.e., 30 and 10 K above T_c, the temperature below which a further increase of the resistivity and of the thermopower is observed. The structural investigation does not reveal any significant structural modifications at T_u. Only the diffuse lines observed inside the Bragg layers perpendicular to c^* seem to disappear around T_u. The first feature recalls the behavior[22,75] found in the $(TMTTF)_2X$ series, where the anomaly in transport measurement was initially believed not to affect the lattice symmetry and was interpreted as a crossover on the charge transport. Actually, recent nuclear magnetic resonance (NMR) detection of a charge disproportionation[18] and the divergence of the dielectric constant[19] were able to show that this anomaly leads to a breaking of the inversion symmetry and that $(TMTTF)_2X$ undergoes a second-order phase transition to a CO ferroelectric ground state. Only very recently, weak variations of the lattice expansion[26] and of the intensity of several Bragg reflections[27] were detected proving that the lattice is also involved in the CO transition of $(TMTTF)_2X$. A similar behavior should occur at T_u in the Cl and Br salts. However, the photographic method used in the present investigation was not adapted to detect small variations of the Bragg intensity (around 10% in the $(TMTTF)_2X$ [27]) and/or possible symmetry breaking of the $I\bar{4}2d$space group element at T_u. In addition, the Cl crystal used was also of poor crystalline quality.

It is however interesting to discuss what kind of symmetry breaking keeping the c translational symmetry in the chain direction (no superlattice reflection is detected at T_u) is expected in $(o\text{-DMTTF})_2X$. The most obvious symmetry breaking compatible with the appearance of a gap of charge in the transport properties without any appreciable change in the spin degrees of freedom (i.e., the spin susceptibility) and the detection of "pretransitional" $4k_F$ fluctuations is the establishment of a $4k_F = c^*$ order (either a $4k_F$ CO or a $4k_F$ BOW) in the stack direction. By examining the structure shown Fig. 1, such a $4k_F$ order must obviously break the screw axis symmetry 2_1 of the stack itself. However, the $4k_F$ order must also break either one set of two-fold symmetry axis running along a or b in the $I\bar{4}2d$space group or both. This symmetry operation involves the different stacks of the unit cell. Let us consider the break of only one set of twofold axis symmetry (let us say, along a). Figure 1 shows that such a set of binary axis is located in the molecular plane and directed along the long direction of the *o*-DMTTF molecule of one stack out of two (let us say, stack I) and is located midway between two molecules and directed along the short molecular direction of the other stack (let us say, stack II). The breaking of the twofold symmetry along a thus leads to a dimerization of stack I (but all the molecules remain equivalent by the presence of the twofold axis symmetry along b). This corresponds to a $4k_F$ BOW of the stack I. In addition, the same symmetry breaking also leads to inequivalent molecules in stack II (however, the intermolecular distances remain uniform by the presence of the twofold axis symmetry along b). This corresponds to a $4k_F$ CO of the stack II. In other words, the symmetry breaking of one set of twofold symmetry axis leads to the coexistence of $4k_F$ bond (DM) and $4k_F$ site (CO) modulations on the differently oriented stacks I and II, respectively. However, these symmetry considerations do not fix the relative amount between the CO and DM orders. At these different CO and DM structural orders will correspond gaps of charge of different magnitude. The smallest gap will condition transport properties below T_u. These $4k_F$ orders of different symmetry will also break other symmetry elements relating the different stacks such as the diamond glide plane symmetry d and the fourfold screw axis symmetry -4. The breaking of the -4 symmetry will yield to nonequivalent molecular charges in the tetrahedral environment of the anion. This effect must lead to a shift of the anion from its high-temperature symmetric position. This coexistence of both DM and CO in the same structure bears some resemblance with the one found for the $4k_F$ order of $(DI\text{-}DCNQI)_2Ag$, which also breaks a fourfold symmetry axis.[33] There are two ways to break one set of twofold axis symmetry: either by breaking the binary axis directed along a or the one directed along b. In

that case, the tetragonal symmetry is lowered to a monoclinic symmetry compatible with ferroelectricity. Another possibility will be the simultaneous symmetry breaking of the two sets of twofold axis symmetry both along a and b. In that case, each stack will present a mixture of DM and CO $4k_F$ orders. It is however important to notice that a recent Raman and infrared investigation[65] has not detected any evidence of CO. This feature together with the observation of $4k_F$ pretransitional diffuse lines discussed in the last section suggests that the DM counterpart at the $4k_F$ order should be the dominant one. The presence of DM chains with a more conducting character could also explain that the increase of resistivity below T_u is soft.

C. The T_c transition

In the low-pressure region, a clear phase transition is observed at $T_c \approx 50$ K in the Cl and Br salts by all experimental techniques from a nonmetallic state toward a clearly insulating state. The observation of $2k_F$ satellites reflections in the x-ray patterns is a signature of the establishment of a structural modulation at T_c. The stabilization of the wave vector component $1/2c^*$ means that a tetramerization (BOW) of the molecular stacks occurs. The $2k_F$ BOW order can be due either to a Peierls instability or to a SP instability, depending upon the importance of electron-electron correlations of the electron gas. In order to deepen this point, let us now discuss the nature of the electronic ground state. As already explained before, the activation energy is difficult to extract from resistivity, ESR, and SQUID data. Nevertheless, the activation energy extracted from longitudinal resistivity data at low pressure around 30 K [see inserts of Figs. 3(a) and 4(a)] is around 200 K for Cl and 400 K for Br, which gives a gap for the charge degrees of freedom $\Delta_\rho \approx 400$ K for Cl and 800 K for Br, which is much larger than $\Delta_\rho \approx 190$ K for the spin degrees of freedom. This difference, indicating a certain decoupling between charge and spin degrees of freedom, is a proof of the presence of substantial electron-electron repulsions in the $(o\text{-DMTTF})_2X$ series. Indeed, for a standard $2k_F$ BOW Peierls transition in a weakly correlated electron gas, one obtains $\Delta_\rho \approx \Delta_\sigma$, as found, for example, at the Peierls transition of TSF-TCNQ ($\Delta_\rho \approx \Delta_\sigma \approx 110$ K.[76,77]). Differently, the picture of a SP transition leading to the pairing of the spins is justified if the charge degrees of freedom are frozen (i.e., if $\Delta_\rho > > \Delta_\sigma$). This is the case of $(BCPTTF)_2PF_6$ and AsF_6, where $\Delta_\rho \approx 1000$ K and $\Delta_\sigma \approx 100$ K,[78] and of $(TMTTF)_2PF_6$ and AsF_6, where $\Delta_\rho \approx 600$ K[22,61] and $\Delta_\sigma \approx 75$ K.[20] $(o\text{-DMTTF})_2X$ presents an intermediate situation between the pure Peierls and SP scenario with a ratio $\Delta_\rho/\Delta_\sigma = 2-4$ similar to the one ($\Delta_\rho \approx 225$ K/$\Delta_\sigma \approx 80$ K) ≈ 2.8[76,79] measured below 38 K in the TTF stack of TTF-TCNQ. TTF-TCNQ is a correlated metal,[16,62] where both the divergence of the $2k_F$ and $4k_F$ CDW instabilities can be accounted for by the Tomonaga-Luttinger parameter $K_\rho \sim 0.3$.[80] This means that, in the $2k_F$ phase, $(o\text{-DMTTF})_2X$ should bear some resemblance to the low-temperature phase of TTF-TCNQ, although the activation energies are two to four times larger in the former compound. However, because of the presence of a high-temperature $4k_F$ charge localization transition, we chose to call SP the $2k_F$ BOW order in the low-pressure range of the phase diagram (Fig. 16).

The determination of the $2k_F$ modulated structure stabilized below T_c, and in particular the determination of the phase shift between the tetramerized stacks, requires a refinement that goes beyond the present study. This structural determination should however be quite delicate. The main reason is that, if one ignores an eventual change of space group at T_u, the order parameter has four components because there are four nonequivalent critical wave vectors able to achieve the T_c transition: (1/2, 0, 1/2), (1/2, 0, −1/2), (0, 1/2, 1/2), and (0, 1/2, −1/2). And the number of them that condense below T_c, in order to set the modulation pattern, is unknown. The theory of the phase transitions governed by an order parameter with four components is quite subtle[81,82] because such a four-component order parameter-driven phase transition can either be continuous (second order) or discontinuous (first order). With the present space group symmetry and critical wave vectors, renormalization group calculations[81] show the occurrence of a continuous transition, in agreement with the experimental observations. The number of wave vector components that condense in the modulated structure, and thus the symmetry of the resulting Bravais lattice, depends upon the relative values and signs of the coefficients of the Landau development given in Ref. 82. Finally as for the T_u transition, the $2k_F$ distortion stabilized below T_c is not necessarily identical for all the stacks. In particular the DM stack should undergo a stronger SP instability than the CO stack.

In the present case, the mean-field thermal dependence of the superstructure satellite intensity (Fig. 15), related to the square of the order parameter, shows the occurrence of a second-order transition for the I salt that does not present the T_u anomaly. Figure 15 also shows that, as the T_u transition grows along the sequence Br, Cl, the thermal dependence of the order parameter becomes steepest at T_c. The thermal dependence measured for the Cl salt is close to that expected in the vicinity of a tricritical point. This implies a significant coupling between the order parameters of the T_c and T_u transitions. The polynomial dependence of the order parameters in this coupling term cannot be determined because the symmetry breaking at T_u is unknown.

D. Phase diagram

From our results, Fig. 16 presents a generic phase diagram for the Cl and Br salts, with the origin of pressure for the Cl salt and a pressure shift of 3.5 kbar for the Br one. In the high-temperature regime, a metal-to-insulator crossover is observed below T_ρ. Below a critical pressure, $P_c \approx 7$ kbar, a net charge localization appears at T_u followed, at T_c, by a phase transition stabilizing a $2k_F$ order. At 7 kbar, the T_u and T_c lines appear to merge together. Above 7 kbar, T_c decreases, reaching 25 K at 18 kbar. The observation of a metallic state in the transverse resistivity is concomitant to the merging of the T_u line, which allows us to consider that T^* is the onset of the deconfinement of the carriers, i.e., the crossover between a 1D metal at high temperature and a 3D metal establishing progressively when cooling down. Due to its tetragonal structure, the $(o\text{-DMTTF})_2X$ family undergoes directly a 1D-3D crossover at variance with

triclinic $(TMTTF)_2X$ salts where an intermediate 2D regime is observed.[83,84]

The 1D regime in the phase diagram is then located above the two lines T_ρ (P) and T^* (P). This is the region where we could evaluate the Luttinger exponent K_ρ from the temperature dependence of the longitudinal resistivity. However, to do that, we need to correct the raw data, which are constant pressure data, in order to get constant volume data, as we did for $(TMTSF)_2PF_6$.[84] The pressure and temperature dependences of the lattice parameter along the chain together with the pressure dependence of the longitudinal conductivity at different temperatures, which are necessary to perform this correction are unknown for the $(o\text{-DMTTF})_2X$ salts and certainly different from those determined for the $(TMTSF)_2X$ salts. This is the reason why we do not give any estimation for K_ρ.

The nature of the $4k_F$ structural order accompanying the charge localization is not yet determined. If such structural order exists, it must be a mixture of CO and DM as deduced from symmetry considerations. However, the absence of CO features in optical measurements[65] means that the amplitude of the CO counterpart at the $4k_F$ order must be particularly weak. This is consistent with the fact that T_c is nearly independent of the pressure below $P_c = 7$ kbar (Fig. 16). If a strong CO component was stabilized at T_u, one should observe, in the phase diagram, a concomitant increase of T_c with the decrease of T_u. The repulsion between the CO and the $2k_F$ BOW orders is due to heteropolar charge configurations induced by the CO phase that kill the $2k_F$ BOW instability. This effect has been previously observed for the AO transition in the $[(TMTSF)_{1-x}(TMTTF)_x]_2ReO_4$ solid solution[48] and for the SP transition in $(TMTTF)_2AsF_6$ under pressure[85] and confirmed by the numerical simulations of Ref. 15. In addition, the threshold field for depinning of the ordered state is very weak below P_c. This is in sharp contrast with measurements of large threshold fields in the CO phase of the order of several hundreds of V/cm in α-$(BEDT\text{-}TTF)_2I_3$[86] or in θ-$(BEDT\text{-}TTF)_2CsCo(SCN)_4$[87] but in agreement with the coexistence of CO/DM with a SP order.

Above the deconfinement pressure, P_c, the low-temperature ordered phase is certainly a $2k_F$ ordered state even if there is not enough data to conclude firmly. Nevertheless, the low value of the measured threshold field is consistent with the existence of a Peierls (CDW/BOW) ground state related to a nesting of Fermi surface, similarly to the δ-$(EDT\text{-}TTF\text{-}CONMe_2)_2X$ case.[23]

As mentioned earlier, the I salt is very particular and hard to place on the phase diagram even if it presents similar features to the other compounds of the family. Indeed, resistivity and ESR data give a poorly defined T_c for the $2k_F$ transition, which contrasts with the x-ray data showing a well-defined second-order phase transition, at a well-defined $T_c \approx 48$ K, stabilizing a $2k_F$ long-range order (at the scale of the experimental resolution). No signature of an intermediate phase is visible. For this reason, one would place the I salt at ambient pressure on the right part of the phase diagram (Fig. 16) above the critical pressure. More precisely, it would be equivalent to the Cl salt under an approximate applied pressure of 9 kbar, considering only the value of T_c. Surprisingly, this anionic pressure sequence along the phase diagram is contrary to the expected chemical pressure related to the size of the halogen anion increasing along the sequence I, Br, Cl.

This so-called "normal" chemical pressure effect, related to a contraction of the cell upon introduction of smaller anions, is indeed observed in the $(TMTTF)_2X$ series,[16] where the anion is only weakly bound to the surrounding TMTTF molecules. On the other hand, the κ phases of BEDT-TTF, formulated as κ-$(BEDT\text{-}TTF)_2[Cu(N(CN)_2)]X$, $X = Cl, Br, I$[88] exhibit what would be described as a negative chemical pressure effect. Its origin can be related to the well-defined interaction of the halide anion with the anionic sublattice. The negative pressure effect observed here in the $(o\text{-DMTTF})_2X$ series thus indicates that the halide anions in these phases are also engaged in specific intermolecular interactions, actually directional C-H$\bullet\bullet\bullet X$ hydrogen bonds involving the methyl groups of the DMTTF molecule.[51,65] Thus, these interactions probably control the anisotropy of compressibility and the observed pressure dependence.

It is thus possible that the much larger size of the iodine anion with respect to the light chlorine and bromine anions should modify the fine structure of the phase diagram as the interaction of the conducting stack with the anionic potential may be also considered. The presence of a strong anionic potential may also limit the thermal contraction of the stack upon cooling, which favors the charge localization. The iodine anion could also induce disorder in the structure, which explains that the T_ρ of localization remains at high temperature even under high pressures. However, this disorder, if it exists, is not strong enough to kill the divergence of the $2k_F$ fluctuations at T_c as sharp satellite reflections of comparable intensity with the Br and Cl salts, are observed. It can however induce inhomogeneities in the modulated structure such as a texture of metallic filaments whose effect will be to smooth the electronic singularities at T_c.

In conclusion, using a set of different experimental techniques, we were able to construct a generic (pressure, temperature) phase diagram for the quarter-filled-band family $(o\text{-DMTTF})_2X$, where X is a halogen. This phase diagram, which shows a subtle coexistence between $4k_F$ and $2k_F$ phenomena, with the vanishing of $4k_F$ effects under pressure accompanied by a crossover from a SP to a Peierls ground state (both ground states having the same order parameter symmetry), seems to be driven by the electron-electron interactions. In this respect, the observed properties resemble those of the $(DMe\text{-}DCNQI)_2X$ series, which presents a coexistence of both kinds of instabilities, but contrast with those of the δ-$(EDT\text{-}TTF\text{-}CONMe_2)_2X$ family, where there is segregation between the CO and the $2k_F$ Peierls orders. This difference could be explained by the fact that the DM order dominates in the $(o\text{-DMTTF})_2X$ and $(DMe\text{-}DCNQI)_2X$, while the CO counterpart dominates in δ-$(EDT\text{-}TTF\text{-}CONMe_2)_2X$. Further experiments are, however, necessary to confirm these findings.

ACKNOWLEDGMENTS

The authors acknowledge ANR "three-quarter-filled" (ANR-08-BLAN-0140) for financial support and E. Attie and A. Benallouche for their help during the ESR and x-ray measurements. G. Guillier and D. Petermann are acknowledged for their technical support concerning the x-ray diffraction set-up, and E. W. Reinheimer and A. Assaf (Rennes) for sample preparation.

*pascale.foury@u-psud.fr

[1] *Physics and Chemistry of Low Dimensional Inorganic Conductors*, edited by C. Schlenker, J. Dumas, M. Greenblatt, and S. van Smaalen (Plenum Publishing Corporation, New York, 1996), Vol. 354.

[2] P. Batail (ed.), Chem. Rev. **104**, 4887 (2004).

[3] S. Kagoshima, K. Kanoda, and T. Mori (eds.), J. Phys. Soc. Jpn. **75**, 051001 (2006).

[4] F. Castet, A. Fritsch, and L. Ducasse, J. Phys. I France **6**, 583 (1996); L. Cano-Cortés, A. Dolfen, J. Merino, J. Behler, B. Delley, K. Reuter, and E. Koch, Eur. Phys. J. B **56**, 173 (2007); L. Cano-Cortés, A. Dolfen, J. Merino, and E. Koch, Physica **405**, S185 (2010).

[5] J. Kondo and K. Yamaji, J. Phys. Soc. Jpn. **43**, 424 (1977); J. Hubbard, Phys. Rev. B **17**, 494 (1978).

[6] J. P. Pouget, S. K. Khanna, F. Denoyer, R. Comès, A. F. Garito, and A. J. Heeger, Phys. Rev. Lett. **37**, 437 (1976).

[7] J. P. Pouget, in *Physics and Chemistry of Low Dimensional Inorganic Conductors*, edited by C. Schlenker, J. Dumas, M. Greenblatt, and S. van Smaalen (Plenum Publishing Corporation, New York, 1996), Vol. 354, pp. 187–219.

[8] D. E. Moncton, R. J. Birgeneau, L. V. Interrante, and F. Wudl, Phys. Rev. Lett. **39**, 507 (1977).

[9] M. Nakamura, Phys. Rev. B **61**, 16377 (2000); P. Sengupta, A. W. Sandvik, and D. K. Campbell, *ibid.* **65**, 155113 (2002); M. Tsuchiizu and A. Furusaki, *ibid.* **69**, 035103 (2004).

[10] Z. G. Soos, M. Kumar, S. Ramasesha, and R. A. Pascal Jr., Physica B **405**, S353 (2010).

[11] Y. Nogami, T. Kambe, N. Fujimura, K. Oshima, T. Mori, and T. Kawakubo, Synthetic Metals **135-136**, 637 (2003); T. Takahashi, Synth. Met. **133-134**, 261 (2003).

[12] V. J. Emery, R. Bruinsma, and S. Barisic, Phys. Rev. Lett. **48**, 1039 (1982).

[13] F. Mila and X. Zotos, Europhys. Lett. **24**, 133 (1993).

[14] V. J. Emery and C. Noguera, Phys. Rev. Lett. **60**, 631 (1988); R. T. Clay, S. Mazumdar, and D. K. Campbell, Phys. Rev. B **67**, 115121 (2003); S. Ejima, F. Gebhard, S. Nishimoto, and Y. Ohta, *ibid.* **72**, 033101 (2005).

[15] M. Kuwabara, H. Seo, and M. J. Ogata, J. Phys. Soc. Jpn. **72**, 225 (2003).

[16] D. Jérome, Chem. Rev. **11**, 5565 (2004).

[17] B. Dumoulin, PhD thesis of physics, Université de Sherbrooke, Canada (1997).

[18] D. S. Chow, F. Zamborszky, B. Alavi, D. Tantillo, A. Baur, C. A. Merlic, and S. E. Brown, Phys. Rev. Lett. **85**, 1698 (2000).

[19] P. Monceau, F. Y. Nad, and S. Brazovskii, Phys. Rev. Lett. **86**, 4080 (2001).

[20] J. P. Pouget, P. Foury-Leylekian, D. Le Bolloc'h, B. Hennion, S. Ravy, C. Coulon, V. Cardoso, and A. Moradpour, J. Low Temp. Phys. **142**, 147 (2006).

[21] S. Huizinga, J. Kommandeur, G. A. Sawatzky, B. T. Thole, K. Kopinga, W. J. M. de Jonge, and J. Roos, Phys. Rev. B **19**, 4723 (1979).

[22] R. Laversanne, C. Coulon, B. Gallois, J. P. Pouget, and R. Moret, J. Phys. Lett. **45**, L393 (1984).

[23] P. Auban-Senzier, C. R. Pasquier, D. Jérome, S. Suh, S. E. Brown, C. Mézière, and P. Batail, Phys. Rev. Lett. **102**, 257001 (2009).

[24] S. Brazovskii, Synth. Met. **133-134**, 301 (2003).

[25] J. Riera and D. Poilblanc, Phys. Rev. B **63**, 241102(R) (2001).

[26] M. de Souza, P. Foury-Leylekian, A. Moradpour, J.-P. Pouget, and M. Lang, Phys. Rev. Lett. **101**, 216403 (2008).

[27] P. Foury-Leylekian, S. Petit, G. Andre, A. Moradpour, and J. P. Pouget, Physica B **405**, S95 (2010)

[28] L. Zorina, S. Simonov, C. Mézière, E. Canadell, S. Suh, S. E. Brown, P. Foury-Leylekian, P. Fertey, J.-P. Pouget, and P. Batail, J. Mater. Chem. **19**, 6980 (2009).

[29] V. Ilakovac, S. Ravy, J. P. Pouget, W. Reiss, W. Brutting, and M. Schwoerer, J. Physique IV **3**, C2-137 (1993).

[30] F. Goze, A. Audouard, L. Brossard, V. N. Laukhin, J. P. Ulmet, M. L. Doublet, E. Canadell, J. P. Pouget, V. E. Zavodnik, R. P. Shibaeva, B. Hilti, and C. W. Mayer, Synth. Met. **70**, 1279 (1995); Physica B **211**, 286 (1995).

[31] R. Moret, J. P. Pouget, R. Comès, and K. Bechgaard, Phys. Rev. Lett. **49**, 1008 (1982).

[32] S. Aoyagi, K. Kato, A. Ota, H. Yamochi, G. Saito, H. Suematsu, M. Sakata, and M. Takata, Angew. Chem. Int. Ed. **43**, 3670 (2004).

[33] T. Kakiuchi, Y. Wakabayashi, H. Sawa, T. Itou, and K. Kanoda, Phys. Rev. Lett. **98**, 066402 (2007).

[34] K. Penc and F. Mila, Phys. Rev. B **50**, 11429 (1994).

[35] C. Coulon, P. Vaca, T. Granier, and B. Gallois, Synth. Met. **27**, B449 (1988).

[36] R. Laversanne, C. Coulon, J. Amiell, and J. P. Morand, Europhys. Lett. **2**, 401 (1986).

[37] P. Vaca, C. Coulon, S. Ravy, J. P. Pouget, and J. M. Fabre, J. Phys. I France **1**, 125 (1991); M. Fourmigué, E. W. Reinheimer, A. Assaf, O. Jeannin, A. Saad, P. Auban-Senzier, P. Alemany, A. Rodriguez-Fortea, and E. Canadell, Inorg. Chem. **50**, 4171 (2011).

[38] Q. Liu, S. Ravy, J. P. Pouget, C. Coulon, and C. Bourbonnais, Synth. Met. **56**, 1840 (1993).

[39] S. Hünig and E. Herverth, Chem. Rev. **104**, 5535 (2004).

[40] H. P. Werner, J. U. Von Schütz, H. C. Wolf, R. Kremer, M. Gehrke, A. Aumüller, P. Erk, and S. Hünig, Solid State Commun. **65**, 809 (1988).

[41] R. Moret, P. Erk, S. Hünig, and J. U. Von Schütz, J. Phys. France, **49**, 1925 (1988).

[42] K. I. Hiraki and K. Kanoda, Phys. Rev. B **54**, 17276 (1996).

[43] Y. Nogami, R. Moret, J. P. Pouget, Y. Yamamoto, K. Oshima, K. Hirati, and K. Kanoda, Synth. Met. **102**, 1778 (1999).

[44] K. I. Hiraki and K. Kanoda, Phys. Rev. Lett. **80**, 4737 (1998).

[45] T. Itou, K. Kanoda, K. Murata, T. Matsumoto, K. Hiraki, and T. Takahashi, Phys. Rev. Lett. **93**, 216408 (2004).

[46] T. Itou, K. Kanoda, K. Hiraki, T. Takahashi, K. Murata, and T. Matsumoto, Phys. Rev. B **72**, 113109 (2005).

[47] K. Heuzé, M. Fourmigué, P. Batail, C. Coulon, R. Clérac, E. Canadell, P. Auban-Senzier, S. Ravy, and D. Jérome, Adv. Mater. **15**, 1251 (2003).

[48] V. Ilakovac, S. Ravy, J. P. Pouget, C. Lenoir, K. Boubekeur, P. Batail, S. D. Babic, N. Biskop, B. Korin-Hamzic, S. Tomic, and C. Bourbonnais, Phys. Rev. B **50**, 7136 (1994).

[49] S. Biermann, A. Georges, A. Lichtenstein, and T. Giamarchi, Phys. Rev. Lett. **87**, 276405 (2001).

[50] A. Abderraba, R. Laversanne, E. Dupart, C. Coulon, P. Delhaes, and C. Hauw, J. Phys. Colloq. **44**, C3-1243 (1983).

[51] M. Fourmigué, E. W. Reinheimer, K. R. Dunbar, P. Auban-Senzier, C. Pasquier, and C. Coulon, Dalton Trans., 4652 (2008).

[52]N. Kang, P. Auban-Senzier, C. R. Pasquier, Z. A. Ren, J. Yang, G. C. Che, and Z. X. Zhao, New J. Phys. **11**, 025006 (2009).
[53]J. Moser, M. Gabay, P. Auban-Senzier, D. Jérome, K. Bechgaard, and J. M. Fabre, Eur. Phys. J. B **1**, 39 (1998).
[54]K. Murata, H. Yoshino, H. Om Yadav, Y. Honda, and N. Shirakawa, Rev. Sci. Instrum. **68**, 2490 (1997).
[55]K. Bechgaard, C. S. Jacobsen, K. Mortensen, H. J. Pedersen, and N. Thorup, Solid State Commun. **33**, 1119 (1980).
[56]K. Mortensen, E. M. Conwell, and J. M. Fabre, Phys. Rev. B **28**, 5856 (1983).
[57]P. M. Chaikin, J. F. Kwak, T. E. Jones, A. F. Garito, and A. J. Heeger, Phys. Rev. Lett. **31**, 601 (1973).
[58]F. J. Adrian, Phys. Rev. B **33**, 1537 (1986).
[59]Y. Tomkievicz, B. C. Scott, L. J. Tao, and R. S. Title, Phys. Rev. Lett. **32**, 1363 (1974).
[60]C. Coulon and R. Clérac, Chem. Rev. **104**, 5655 (2004).
[61]C. Coulon, G. Lalet, J. P. Pouget, P. Foury-Leylekian, A. Moradpour, and J. M. Fabre, Phys. Rev. B **76**, 085126 (2007).
[62]J. P. Pouget, in *Semiconductors and Semimetals*, edited by E. M. Conwell (Academic Press, Boston, 1988), Vol. 27, pp. 87–215.
[63]Y. Bouveret and S. Megtert, J. Phys. France **50**, 1649 (1989).
[64]The continuous lines of Fig. 15 have been obtained with the simplest phenomenological free energy, including a coupling term Γ able to induce a first-order transition (for example a magnetoelastic coupling in the case of a magnetic transition): $\frac{F}{N} = -\frac{k_B T_c}{2} m^2 - \frac{\Gamma}{4} m^4 + k_B T[\frac{1+m}{2} \ln(\frac{1+m}{2}) + \frac{1-m}{2} \ln(\frac{1-m}{2})]$. After minimization of the free energy and by introducing the reduced quantities $\alpha = \frac{\Gamma}{k_B T_c}$ and $\tau = \frac{T}{T_c}$, the thermal dependence of the order parameter m is given by $m = \tanh[\frac{m+\alpha m^3}{\tau}]$. $\alpha = 0$ corresponds to a second-order transition, while $\alpha = 1/3$ to a tricritical point.
[65]D. Jankowski, R. Świetlik, E. W. Reinheimer, and M. Fourmigué, J. Raman Spectrosc. **42**, 1518 (2011).
[66]J. P. Pouget and S. Ravy, Synth. Met. **85**, 1523 (1997).
[67]J. P. Pouget, Chem. Scr. **17**, 85 (1981).
[68]J. P. Pouget, R. Moret, R. Comès, K. Bechgaard, J. M. Fabre, and L. Giral, Mol. Cryst. Liq. Cryst. **79**, 129 (1982).
[69]S. Kagoshima, J. P. Pouget, T. Yasunaga, and J. B. Torrance, Solid State Comm. **46**, 521 (1983).
[70]K. Mortensen, C. S. Jacobsen, A. Lindegaard-Andersen, and K. Bechgaard, J. Phys. Colloq. **44**, C3-1349 (1983).
[71]C. Rovira, J. Tarres, J. Llorca, E. Molins, J. Veciana, S. Yang, D. O. Cowan, C. Garrigou-Lagrange, J. Amiell, P. Delhaes, E. Canadell, and J. P. Pouget, Phys. Rev. B **52**, 8747 (1995).
[72]A. J. Epstein, J. S. Miller, J. P. Pouget, and R. Comès, Phys. Rev. Lett. **47**, 741 (1981).
[73]C. Coulon, P. Delhaes, J. Amiell, J. P. Manceau, J. M. Fabre, and L. Giral, J. Phys. (Paris) **43**, 1721 (1982).
[74]J. P. Pouget, R. Moret, R. Comès, G. Shirane, K. Bechgaard, and J. M. Fabre, J. Phys. Colloq. **44**, C3-969 (1983).
[75]C. Coulon, S. S. P. Parkin, and R. Laversanne, Phys. Rev. B **31**, 3583 (1985).
[76]S. Etemad, Phys. Rev. B **13**, 2254 (1976).
[77]L. I. Buravov, R. N. Lyubovskaya, R. B. Lyubovskii, and M. L. Khidekel, Sov. Phys. JETP **43**, 1033 (1977); J. C. Scott, S. Etemad, and E. M. Engler, Phys. Rev. B **17**, 2269 (1978).
[78]L. Ducasse, C. Coulon, D. Chasseau, R. Yagbasan, J. M. Fabre, and A. K. Gousmia, Synth. Met. **27**, B543 (1988); Δ_σ (unpublished result of C. Coulon) is given in J.-P. Pouget, Eur. Phys. J. B **24**, 415 (2001).
[79]T. Takahashi, D. Jérome, F. Masin, J. M. Fabre, and L. Giral, J. Phys. C **17**, 3777 (1984).
[80]B. Dumoulin, J. P. Pouget, and C. Bourbonnais, Synth. Met. **103**, 1797 (1999).
[81]J. C. Tolédano, L. Michel, P. Tolédano, and E. Brézin, Phys. Rev. B **31**, 7171 (1985).
[82]J. S. Kim, H. T. Stokes, and D. M. Hatch, Phys. Rev. B **33**, 6210 (1986).
[83]P. Auban-Senzier, D. Jérome, C. Carcel, and J.-M. Fabre, J. Phys IV France **114**, 41 (2004).
[84]P. Auban-Senzier, D. Jérome, and J. Moser, in *Physical Phenomena at High Magnetic Field III*, edited by Z. Fisk, L. Gorkov, and R. Schrieffer (World Scientific, Singapore, 1999), p. 211.
[85]F. Zamborszky, W. Yu, W. Raas, S. E. Brown, B. Alavi, C. A. Merlic, and A. Baur, Phys. Rev. B **66**, 081103 (2002).
[86]K. Tamura, T. Ozawa, Y. Bando, T. Kawamoto, and T. Mori, Appl. Phys. Lett. **107**, 103716 (2010).
[87]F. Sawano, I. Terasaki, H. Mori, T. Mori, M. Watanabe, N. Ikeda, Y. Nogami, and Y. Noda, Nature **437**, 522 (2005).
[88]H. Mayaffre, PhD thesis of physics, Université Paris-Sud (1995); K. Miyagawa, K. Kanoda, and A. Kawamoto, Chem. Rev. **104**, 5635 (2004).